The Antarctica component of postglacial rebound model ICE-6G_C (VM5a) based on GPS positioning, exposure age dating of ice thicknesses, and relative sea level histories

Donald F. Argus,[1] W. R. Peltier,[2] R. Drummond[2] and Angelyn W. Moore[1]

[1]*Jet Propulsion Laboratory, California Institute of Technology, Pasadena, CA 91109, USA. E-mail: Donald.F.Argus@jpl.nasa.gov*
[2]*Department of Physics, University of Toronto, ON M5S 1A7, Canada*

SUMMARY

A new model of the deglaciation history of Antarctica over the past 25 kyr has been developed, which we refer to herein as ICE-6G_C (VM5a). This revision of its predecessor ICE-5G (VM2) has been constrained to fit all available geological and geodetic observations, consisting of: (1) the present day uplift rates at 42 sites estimated from GPS measurements, (2) ice thickness change at 62 locations estimated from exposure-age dating, (3) Holocene relative sea level histories from 12 locations estimated on the basis of radiocarbon dating and (4) age of the onset of marine sedimentation at nine locations along the Antarctic shelf also estimated on the basis of ^{14}C dating. Our new model fits the totality of these data well. An additional nine GPS-determined site velocities are also estimated for locations known to be influenced by modern ice loss from the Pine Island Bay and Northern Antarctic Peninsula regions. At the 42 locations not influenced by modern ice loss, the quality of the fit of postglacial rebound model ICE-6G_C (VM5A) is characterized by a weighted root mean square residual of 0.9 mm yr^{-1}. The Southern Antarctic Peninsula is inferred to be rising at 2 mm yr^{-1}, requiring there to be less Holocene ice loss there than in the prior model ICE-5G (VM2). The East Antarctica coast is rising at approximately 1 mm yr^{-1}, requiring ice loss from this region to have been small since Last Glacial Maximum. The Ellsworth Mountains, at the base of the Antarctic Peninsula, are inferred to be rising at 5–8 mm yr^{-1}, indicating large ice loss from this area during deglaciation that is poorly sampled by geological data. Horizontal deformation of the Antarctic Plate is minor with two exceptions. First, O'Higgins, at the tip of the Antarctic Peninsula, is moving southeast at a significant 2 mm yr^{-1} relative to the Antarctic Plate. Secondly, the margins of the Ronne and Ross Ice Shelves are moving horizontally away from the shelf centres at an approximate rate of 0.8 mm yr^{-1}, in viscous response to the early Holocene unloading of ice from the current locations of the ice shelf centers. ICE-6G_C (VM5A) fits the horizontal observations well (wrms residual speed of 0.7 mm yr^{-1}), there being no need to invoke any influence of lateral variation in mantle viscosity. ICE-6G_C (VM5A) differs in several respects from the recently published W12A model of Whitehouse *et al.* First, the upper-mantle viscosity in VM5a is 5×10^{20} Pa s, half that in W12A. The VM5a profile, which is identical to that inferred on the basis of the Fennoscandian relaxation spectrum, North American relative sea level histories and Earth rotation constraints, when coupled with the revised ICE-6G_C deglaciation history, fits all of the available constraints. Secondly, the net contribution of Antarctica ice loss to global sea level rise is 13.6 m, 2/3 greater than the 8 m in W12A. Thirdly, ice loss occurs quickly from 12 to 5 ka, and the contribution to global sea level rise during Meltwater Pulse 1B (11.5 ka) is large (5 m), consistent with sedimentation constraints from cores from the Antarctica ice shelf. Fourthly, in ICE-6G_C there is no ice gain in the East Antarctica interior, as there is in W12A. Finally, the new model of Antarctic deglaciation reconciles the global constraint upon the global mass loss during deglaciation provided by the Barbados record of relative sea level history when coupled with the Northern Hemisphere counterpart of this new model.

Key words: Satellite geodesy; Global change from geodesy; Glaciology; Dynamics of lithosphere and mantle; Antarctica.
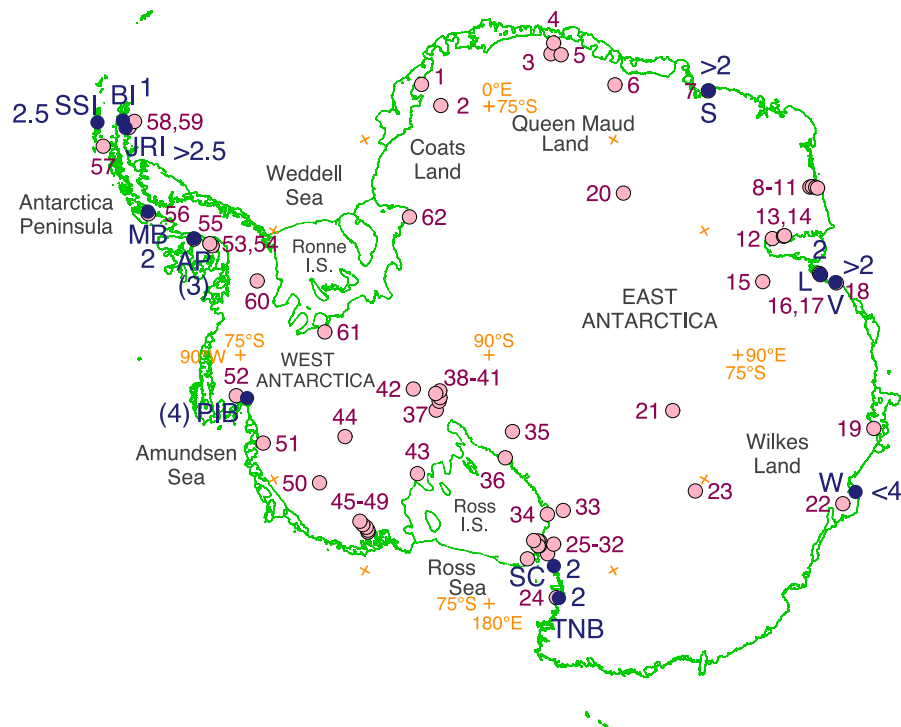
Figure 1. Locations of the 62 ice thickness change data and 12 relative sea level (RSL) histories. The ice thickness change data (pink circles) are from Whitehouse *et al.* (2012a). The RSL data are from this study (Fig. 13). Given for the RSL data (blue circles) is the present rate of RSL decrease in millimetres per year estimated from the youngest sea level marker data available at each site, which are 6–2 ka. Poorly constrained rates of RSL fall are given in parentheses. RSL sites: AP (Ablation Point), BI (Beak Island), JRI (James Ross Island), L (Larsemann), MB (Marguerite Bay), PIB (Pine Island Bay), S (Soya coast), SC (Scott Coast), SSI (South Shetland Islands), TNB (Terra Nova Bay), V (Vestfold hills), W (Windmill islands).

1 INTRODUCTION

The uplift of Antarctica in viscous response to the unloading of ice subsequent to Last Glacial Maximum at 26 ka (Peltier & Fairbanks 2006), and that continued until approximately 4 ka (Peltier *et al.* 2002), is not well constrained by radiocarbon dating of relative sea level (RSL) histories alone, as is the case for both Fennoscandia and Laurentia (e.g. Peltier 1998). (The abbreviation 'ka' is employed herein to indicate thousands of years Before the Present, BP.) Whitehouse *et al.* (2012a) have compiled estimates of ice thickness change during deglaciation of Antarctica based on exposure age dating at 62 locations, thereby usefully enriching the constraints on the deglaciation history that drives the postglacial rebound process of the southern continent (Fig. 1). Moreover, the increasing quantity and quality of GPS observations of vertical motion are also constraining glacial isostatic adjustment in Antarctica (Capra *et al.* 2007; Zanutta *et al.* 2008; Bevis *et al.* 2009; Argus *et al.* 2011; Sjöberg *et al.* 2011; Thomas *et al.* 2011) to a degree that has significantly improved over the past decade.

Furthermore GRACE observations of time-dependent gravity are also providing important constraints on the current rate of loss of grounded ice. However, the accuracy of these estimates depends strongly on the quality of the model of the global process of glacial isostatic adjustment (GIA) that must be employed to decontaminate the gravity observations from the lingering influence of the mass loss that occurred during the last deglaciation event of the current ice-age (e.g. Velicogna & Wahr 2006; Peltier 2009; Shepherd *et al.*, 2012). In this study we will first employ GPS observations of vertical and horizontal crustal motion to estimate the velocities at 59 sites in Antarctica. Vertical rates at the 42 GPS sites recording primarily postglacial rebound are then employed as a primary target for the

revision of the Antarctic component of the previous global model of the GIA process denoted ICE-5G (VM2) that was described in detail in Peltier (2004). The space- and time-dependent ice thickness is adjusted in order to enable the model to best fit the inferred GPS uplift rates as well as the available ice thickness change data of Whitehouse *et al.* (2012a), and 12 of the most useful RSL histories contained in the University of Toronto RSL data base. We then compare the new ICE-6G_C (VM5a) model with the W12A model of Whitehouse *et al.* (2012b) and assess the meaningfulness of the differences. By way of further introduction we will proceed immediately to enumerate the differences we have been led to infer and the fundamental physical reasons that underlie their existence.

Postglacial rebound models consist of three highly correlated characteristics, namely the thickness of the ice sheet as a function of location and time (the glaciation history; Fig. 2), the viscosity of the sublithospheric mantle as a function of depth (Fig. 3), and the thickness of the elastic lithosphere. Errors in the knowledge of deglaciation history, the mantle viscosity profile, or lithospheric thickness may propagate into the inference of the other two parameters. The assumption of lateral homogeneity of the viscoelastic structure may also introduce additional uncertainty.

In constructing the Antarctica component of the new model ICE-6G_C (VM5a), we will continue to assume that the viscoelastic structure may be approximated as spherically symmetric. We will therefore construe the ability of the model to fit the data, subject to this assumption, to constitute a test of the ability of the data to rule out models of this kind. ICE-6G_C (VM5a) is also fit to a wide range of global data and so it will be important to understand that it is not a model which has only local validity. The viscosity of the upper mantle in VM5a is constrained to be $\approx 0.5 \times 10^{21}$ Pa s on the basis of the McConnell (1968) wavenumber spectrum for the time
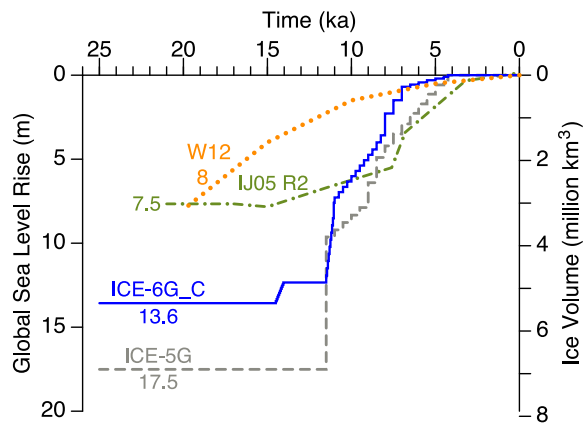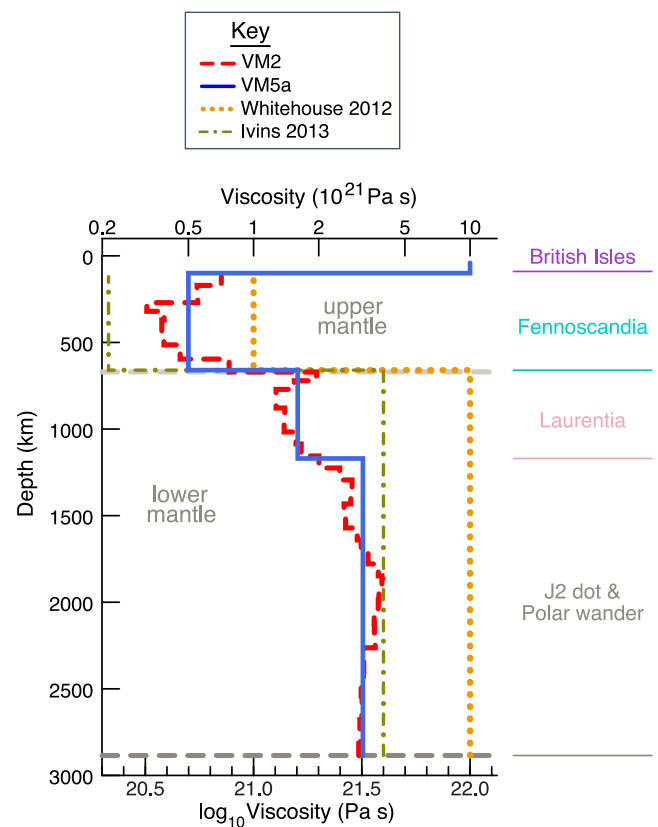
Figure 2. Deglaciation history is compared between four models: ICE-5G (grey; Peltier 2004), ICE-6G_C (blue; this study), W12 (orange; Whitehouse *et al.* 2012a), and IJ05 R2 (olive; Ivins *et al.* 2013). Plotted is Antarctica ice loss (right-hand side axis) and its contribution to global sea level rise (left-hand side axis) as a function of time. The total contribution of Antarctic ice loss to global sea level rise (in m) is given.

Figure 3. Mantle viscosity profile is compared between four models: VM2 (red; Peltier 2004), VM5a (blue; this study), W12A (orange; Whitehouse *et al.* 2012b), and in (olive green; Ivins *et al.* 2013). Relative sea level (RSL) histories from the British Isles are the data most tightly constraining the thickness of the lithosphere to be 90 km. RSL data from Fennoscandia, which has postglacial rebound with a half wavelength of 600 km, constrains the viscosity of the upper mantle to be about 0.5×10^{21} Pa s. RSL data from Laurentia (Canada), which has a postglacial rebound signal with half wavelength about 1500 km constrains the viscosity of the top 500 km of the lower mantle. The postglacial rebound signal in Antarctica has a half wavelength of about 600 km, about the same as Fennoscandia. Therefore, Antarctica viscous response approximately follows that given by the upper-mantle viscosity, that is, 0.5×10^{21} Pa s. Two global geophysical observables, the rate of change of Earth's oblateness (J2 dot) and polar wander, constrain the viscosity of the middle and bottom of the lower mantle.

dependence of viscous uplift of Fennoscandia (Peltier 1996, 2002). This value of upper-mantle viscosity fits all available geologically derived RSL histories, GRACE time-dependent gravity and GPS data in Fennoscandia and Laurentia (Peltier 2004; Paulson *et al.* 2007) given a deglaciation history consistent with geomorphologically inferred limits on the extent of late Pleistocene glaciation (Dyke & Prest 1987).

In this study we aim to test the compatibility of this upper-mantle viscosity value of 0.5×10^{21} Pa s with all available Antarctica GPS, ice thickness change, and RSL data. (Herein we refer to the entire region from the base of the lithosphere to the seismic discontinuity at 660 km as the upper mantle.) We will find that this upper-mantle viscosity structure enables the model to fit all available Antarctica data, a finding that disagrees with a primary conclusion of Whitehouse *et al.* (2012b) that the upper-mantle viscosity in Antarctica must be higher and $\approx 1 \times 10^{21}$ Pa s on the basis of their analysis of the available RSL histories. The ability of ICE-6G_C (VM5a) to fit essentially the same mix of data as that to which W12a has been tuned, in spite of this significant reduction in upper-mantle viscosity, is traceable to two further differences between these two models. First, our lower value of the viscosity of the upper mantle requires that significantly more ice loss must have occurred since Last Glacial Maximum. Given the additional constraints on the timing of the onset of significant ice loss provided by data from sedimentary cores raised from the Antarctic shelf, the deglacial mass loss in the new model is found to be 70 per cent in excess of that in the model of Whitehouse *et al.* (2012a,b). This is helpful in exposing an important source of non-uniqueness in the construction of deglaciation scenarios in circumstances in which there do not exist accurate RSL histories from sites that were once covered by the greatest thicknesses of land ice. For this reason the problem of reconstructing the history of Antarctic ice loss is much more challenging than is the case for either Laurentia or Fennoscandia. In both of these regions the areas of thickest ice cover are now inland seas, respectively, Hudson Bay and the Gulf of Bothnia, the coastlines of which have provided numerous Holocene records of the postglacial emergence of the land that strongly constrain deglaciation history as well as mantle viscosity.

Given that the upper-mantle viscosity in VM5a is half that in W12A (Whitehouse *et al.* 2012b), we find that the characteristic re-

laxation time describing the solid Earth's response to ice unloading in VM5a is approximately half that (≈ 4 kyr) of the characteristic timescale in W12A (≈ 8 kyr; Fig. 4). In this regard it is important to note that the horizontal scale of the most heavily glaciated regions in which excess ice existed at LGM on West Antarctica were of the same scale as the Fennoscandian ice sheet itself (see below). On this basis it is reasonable on *a priori* grounds to expect that the rebound of West Antarctica to load removal will be most sensitive to upper-mantle viscosity just as is the case for Fennoscandia (*cf.* Peltier 1996 for a discussion of the Frechet kernels in terms of which the depth dependence of sensitivity to viscosity variation is quantified). Thus, ICE-6G_C (VM5a) produces current uplift rates which are essentially the same as those characteristic of model W12A because the decrease in characteristic timescale of the rebound process is compensated by the increase in the amount of ice that is lost in deglaciation. Furthermore, the timing of Antarctic deglaciation differs markedly between the two models, such that in ICE-6G_C (VM5a) significant ice loss from Antarctica occurs abruptly
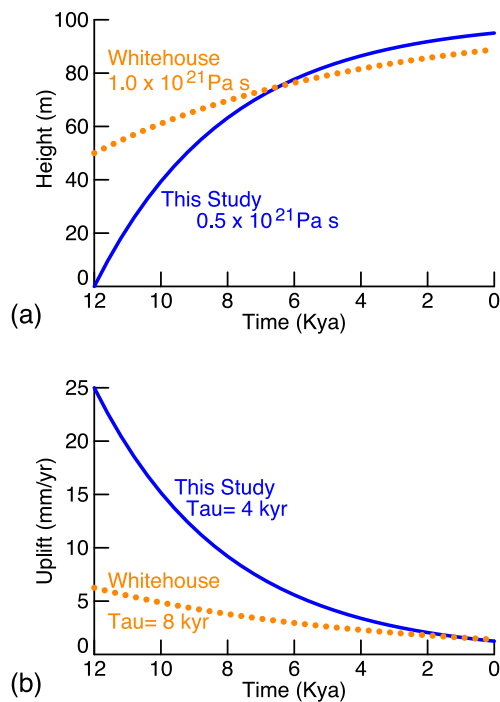
Figure 4. Comparison between the nature of postglacial rebound model in this study (blue) and that in Whitehouse *et al.* (2012b) (orange) in simple formulation (Turcotte & Schubert 2002). The viscosity of the upper mantle in this study (0.5×10^{21} Pa s) is half that in Whitehouse *et al.* (2012b) (1×10^{21} Pa s). Depicted is an example in which models with these two values of viscosity result in the same present uplift rate. In the model like this study the ice sheet (roughly 1000 m thick) lowered Earth's surface 100 m at 12 ka. Earth responds in a viscous manner to unloading of the ice at 12 ka following exponential decay, $100\,\text{m} \times (1 - e^{-t/\tau})$, where *t* is time and τ is 4 kyr. Uplift rate is $25\,e^{-t/\tau}$ and 25 mm yr^{-1} at 12 ka, 9.2 mm yr^{-1} at 8 ka, and 1.2 mm yr^{-1} at present. In the model like Whitehouse *et al.* 2012b the ice sheet at 12 ka is roughly half as thick (500 m) and lowered Earth's surface roughly half as much (50 m) at 12 ka. The characteristic time is twice as long (8 kyr). Present uplift rate is identical (1.2 mm yr^{-1}). Thus Whitehouse *et al.* (2012b) find roughly half the ice loss that we do because they take the mantle viscosity to be twice as high.

at the time of Meltwater Pulse 1B, which is recorded at ∼11.5 ka in Barbados corals at the end of the Younger Dryas cold interval (Peltier & Fairbanks 2006). It is this very early Holocene interval of rapid ice loss that requires model ICE-6G_C (VM5a) to include significantly greater ice loss to fit the totality of the observational constraints.

In contrast, ice loss in model W12A is slow, monotonic, and occurs over the past 20 kyr. In ICE-6G_C, 10 per cent of the total ice loss occurs near the time of Meltwater Pulse 1A (14.5–13.8 ka), 40 per cent occurs near the time of Meltwater Pulse 1B (11.5–11 ka) and 50 per cent occurs from 11 to 4 ka. This ICE-6G_C deglaciation history is consistent with the synthesis of Mackintosh *et al.* (2011) that 'ice retreat in Mac. Robertson Land, East Antarctica, initiated about 14 ka, became widespread about 12 ka, and was completed by 7 ka.' Rapid ice loss from Antarctica at the time of Meltwater Pulse 1B is suggested by the Barbados RSL history and required by sedimentary cores from the continental shelf of Antarctica (E. W. Domack, personal communication 2013; Fig. 5). Seven of 9 ice cores in the illustration indicate the onset of marine sedimentation to be nearer Meltwater Pulse 1B than Meltwater Pulse 1A, and the remaining two cores indicate a time partway between the two meltwater pulses. A small amount of Antarctica ice loss is
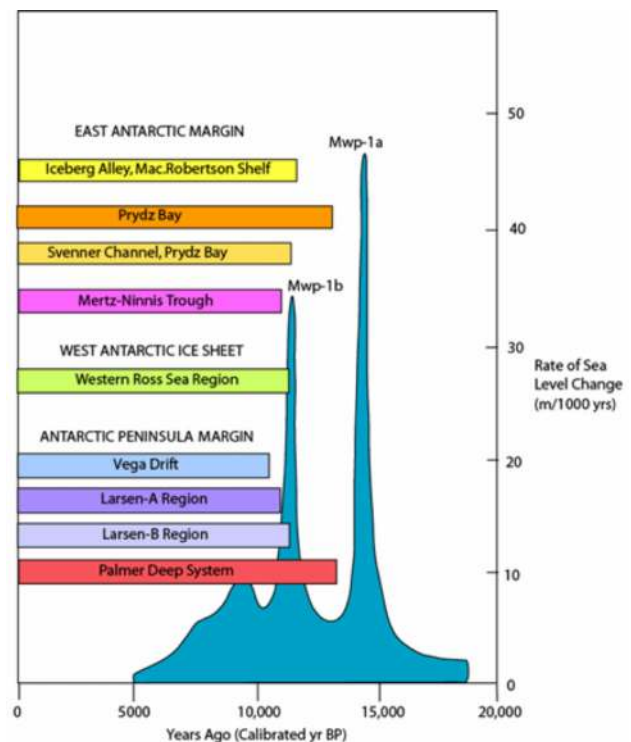
Figure 5. Cores constraining the time of the change of sedimentation from non marine to marine around the continental Antarctic shelf. Illustration courtesy of E. W. Domack (personal communication 2013).

expected to have occurred earlier at the time of Meltwater Pulse 1A (Mackintosh *et al.* 2011), because rapid concurrent ice loss from Laurentia and Fennoscandia quickly raised sea level near Antarctica (Peltier 1999). Stanford *et al.* (2011) maintain that Meltwater Pulses 1A and 1B occurred, respectively, from 14.3 to 12.8 ka and from 11.5 to 8.8 ka (*ca.* Bard *et al.* 2010); ice loss over such longer time periods of pulses of fast ice loss are nevertheless within just 1.5 kyr of those in ICE-6G_C. Using radiocarbon dating, Leventer *et al.* (2006) show that the deposition of varved sediments on calving reentrants along the East Antarctic coast began at ∼11 ka. In ICE-6G_C Antarctica ice loss at the time of Meltwater Pulse 1B is assumed to have raised global eustatic sea level by ≈5 m, contributing to the quick rise in eustatic sea level inferred to have occurred at that time on the basis of Barbados corals (see Peltier 2007, fig. 8). These data constraining the timing of the onset of significant ice loss in Antarctica are critical for eliminating the non-uniqueness in Antarctic deglaciation history that would otherwise remain unresolved. The contribution of Antarctica ice loss to global sea level rise in our new model ICE-6G_C is 13.6 m, less than the 17.5 m in the previous ICE-5G (VM2) model (Peltier 2004), but more than both the 8 m in the W12 model of Whitehouse *et al.* (2012a) and the 7.5 m in the IJ05 R2 model of Ivins *et al.* (2013). Given this brief summary of our results by way of introduction, we proceed in the following sections to provide detailed discussion of the analyses on the basis of which these conclusions have been based.

2 DATA AND METHODS

2.1 Constructing the ICE-6G_C (VM5a) model of postglacial rebound

The methodology that has been employed for construction of the Antarctic component of the ICE-6G (VM5a) model has involved a

number of steps and these have become increasingly complex as this component of the ICE-NG sequence of models has evolved. It will be useful to trace this evolution here. The starting point for the development of this Southern Hemisphere component of the model of global glacial isostatic adjustment was that contained in the ICE-3G (VM1) model of Tushingham & Peltier (1991; hereafter TP91). This was initially based upon the model of Antarctic glaciation history contained in the compilation of Denton & Hughes (1981). Their reconstruction involved a mass loss across the glacial–interglacial transition equivalent to a rise of eustatic sea level of approximately 40 m! In TP91 it was shown that, when the primary Northern Hemisphere ice sheets on Canada and Fennoscandia had their mass and areal extents fixed to enable the GIA model to fit the available RSL histories from the ice covered regions, and the additional constraints provided by Southern Hemisphere sea level data were also invoked (e.g. that from the Wairu Valley of New Zealand), then the timing of deglaciation employed in the Denton and Hughes reconstruction was found to be thousands of years too early. The timing of mass loss was therefore delayed in the ICE-3G reconstruction in order to fit these data and the net mass loss was required to be reduced. However, the regions from which the majority of the mass loss occurred were kept fixed on the basis of the field evidence that had been compiled over at least the previous decade by George Denton, namely the Weddell Sea and Ross Sea embayment regions of West Antarctica. Because the Denton and Hughes reconstruction included the application of a model of ice sheet dynamics the reconstruction was, broadly speaking, consistent with the requirements of rational ice mechanics, at least insofar as these requirements are adequately representable in a model based upon the shallow ice approximation.

Although considerable investment has been made in attempting to ensure that the model ice thickness histories of all of the glaciated regions are equally consistent with such ice mechanical considerations, as the GIA model has evolved (e.g. see Deblonde & Peltier 1991, 1992, 1993; Tarasov & Peltier 1997, 1999, 2002, 2003; Tarasov *et al.* 2012) the need to strictly enforce such consistency has proven to be subject to debate. The issues include the fact that such models of ice sheet dynamics depend upon the availability of sufficiently accurate representations of both climate forcing and subglacial physical processes. The need for a climate derived model of mass balance is clearly problematic for ancient climate regimes and the issue of accurate specification of the boundary conditions at the base of the ice sheet remains unresolved in detail. At least as important as these complexities is the fact that the theoretical formulation of the ice dynamic model itself is a source of significant non-uniqueness. For example, insofar as the latter issue is concerned, if the shallow ice approximation is employed in the theoretical formulation of the ice dynamics model, the model will have limited ability to describe the 'ice streams' and outlet glaciers actually responsible for draining the interior of the ice sheet and that becomes especially important for an ice sheet such as that which covers Antarctica whose interaction with the oceans across the grounding line plays such an important role in ice sheet evolution. Although work is continuing in the community as a whole and in the Toronto group in particular to overcome these problems, the Antarctic reconstruction in the ICE-6G_C (VM5a) model that is under discussion in this paper is based upon the 'GIA only' methodology.

In this methodology the ice thickness history as a function of position is simply adjusted iteratively in order to satisfy all of the available constraints. In the development of the Antarctic component of ICE-6G_C (VM5a), we began with the first guess provided by the precursor ICE-5G (VM2) model. In the first step of iterative refinement, we eliminated entirely the small mass loss from the interior of east Antarctica based upon the inability of the deep ice core records to provide any unambiguous constraint on mass loss from the plateau as a whole. We then adjusted the thickness history of ice cover elsewhere by allowing LGM glacial ice to expand to near the edge of the continental shelf surrounding the continent and then iteratively refined the history of its removal so as to enable the model to fit all available GPS observations of vertical motion of the crust. We sought a model that was minimally perturbed from the precursor model. We therefore retained the property of the earlier model in which it was assumed that the most rapid rate of loss of grounded ice occurred at the time of Meltwater Pulse 1B in the Barbados record at 11.5 ka, the timing of the end of the Younger–Dryas epoch. However, we also allowed an earlier injection of meltwater to derive from Antarctica at the time of Meltwater Pulse 1A. This is expected to have occurred because of the large rise of sea level that would have taken place along coastal Antarctic due to the intense rise of sea level forced by the dominant contribution to Meltwater Pulse 1A from the Laurentide ice sheet complex due to the fact that the gravitationally self-consistent theory of RSL history (e.g. Peltier 1998 for a review) demands that RSL fall in the near field of a deglaciating region and rise in the opposite hemisphere. We expect that the Antarctic contribution to Meltwater Pulse 1A would have derived in significant part from grounded ice that initially covered the continental shelves whereas the contribution to the significantly stronger Meltwater Pulse 1B would have involved the loss of ice from further inland of West Antarctica and from the deep trenches surrounding Antarctica in which the grounded ice would have been especially thick and able to withstand the increase in buoyancy derivative of the Northern Hemisphere contribution of MWP 1A. The only constraint we have on the partition of the mass loss from Antarctica as a whole between the 1A and 1B pulses is that the 1B pulse be sufficiently strong to explain its observed strength in the Barbados coral record of Peltier & Fairbanks (2006). The fact that the 1B pulse did emanate from Antarctica is constrained by the sedimentary core records that have been raised from Antarctic shelf locations (see Mackintosh *et al.* 2011, 2013 for a recent discussion of these records and our further discussion to follow). Following the adjustment of the ice thickness history to enable satisfaction of the totality of the GPS constraints from regions not experiencing modern ice loss (i.e. the Antarctic Peninsula and the Amundsen coastal region of Marie–Byrd Land), the thickness field inferred is smoothed by representing it in terms of the truncated set of spherical harmonics which is required in the theory of global glacial isostatic adjustment. The spatial resolution of the ice thickness field is thereby forced to be consistent with the spatial resolution of the glacial isostatic adjustment model that is employed to predict the rates of vertical crustal motion observed on the GPS receivers for which data is available.

Given this first adjustment to the ice thickness history implied by the fits to the GPS observations, we proceed to further refine the model by subjecting it to the additional set of data that has been provided by the totality of ice thickness constraints available on the basis of exposure age dating of 'trim lines' on erratic boulders and other features that have been interpreted to imply that grounded ice of the dated age was once thick enough so that its upper surface was located at the height of the dated trim line. Of course the locations from which data of this kind is available do not in general correspond to the locations of the GPS receivers from which we have measurements of the vertical motion of the crust. These data therefore provide a set of independent measurements which,

although they are subject to their own issues insofar as interpretation is concerned, are also able to provide estimates of the local history of ice thickness variations, often at several different times from a single localized region. In the next step of iterative refinement, we then, as previously with the GPS data, further adjust the ice thickness history so as to incorporate these additional constraints. We then return to the GPS data to ensure that the additional adjustments required by exposure age dating of erratic trim lines does not require further significant adjustment, and so on iteratively until we arrive at our best possible model. This is the procedure employed in the model construction process.

The ICE-6G_C (VM5a) calculations of the solid Earth's viscoelastic response to the unloading of ice are performed in spectral space using a spherical harmonic representation that is truncated at degree and order 256. Ice thickness change relative to the Present is specified on a Gaussian grid with 256 latitudes and 512 longitudes. The spacing of the grid longitudes is also $0.70°$. At the Equator this is a distance of 78 km, but the distance decreases going toward the North and South poles. In Antarctica the distance is at most 37 km (at $62°S$).

2.2 GPS

The primary basis of the current work consists of the global reanalysis of GPS data for the time period 1994–2012 at the Jet Propulsion Laboratory (Desai *et al.* 2011). Satellite orbits, clocks and site positions on each day have been estimated using models of satellite antenna phase centre variations (Schmid *et al.* 2010; igs08.atx) and solar radiation pressure (Sibthorpe *et al.* 2010). Daily GPS positions are transformed into the ITRF2008 reference frame (Altamimi *et al.* 2011; IGb08) using a scale, a rotation and a translation. The VMF1 troposphere models are employed (Boehm *et al.* 2006a,b, 2007). The solid Earth and pole tide models follow the IERS standards (Petit & Luzum 2010). JPL's GPS estimates of orbits, clocks, and 3000 site positions are available to all at ftp://sideshow.jpl.nasa.gov in the directories JPL_GPS_Products and JPL_GPS_Timeseries/repro2011b.

The estimates of GPS velocity employed herein are, we maintain, more accurate than those employed in previous studies as a consequence of the quality of the JPL reanalysis (Desai *et al.* 2011). The global GPS solution was improved by incorporation of the new model of satellite phase centre variations and the improved model of solar radiation pressure influence. The improved accuracy is evident in the series for Earth's scale used to transform daily GPS positions into ITRF2008 (Argus 2012). In JPL's GPS solution determined 3 yr ago (which was used by Argus *et al.* 2011), the time-series for scale is not particularly 'straight' and implies a 5 mm decrease (of Earth's radius) during 2004 (Fig. S1). In contrast the scale series in the reanalysis (Desai *et al.* 2011) does not suffer from this shortcoming. This indicates that systematic errors due to different phase centre variations in the changing GPS satellite block types have been reduced.

At each of 1000 available global GPS sites we fit estimates of position as a function of time from 1995 to 2012 with a position (at an epoch), a velocity, a sinusoid with a period of 1 yr, and offsets when and where needed. In the present work we have continued to employ the methods we have used on previous occasions (e.g. Argus *et al.* 2010, appendix B). As one part of this methodology we choose whether or not to estimate offsets in a given GPS time-series on the basis of the following four criteria:

(1) whether an estimated offset is larger than 8 mm in the vertical or 3.5 mm in the horizontal,

(2) whether the root mean square misfit decreases by more than 7 per cent by introducing the offset,

(3) whether the offset occurs at the time of a logged antenna substitution and

(4) whether the offset is abrupt.

The threshold values employed (8 mm, 3.5 mm) are those appropriate for the time of a logged antenna substitution but are assumed to be slightly larger (10 mm, 4 mm) if there is no record of an antenna substitution. These criteria are consistent with those that were employed previously in Argus *et al.* (2010), although the improved character of the series allows a 20 per cent reduction in the threshold values for offset estimation.

We placed JPL's GPS results into a global reference frame following the methods of Argus *et al.* (1999, 2010) and Argus & Peltier (2010). Although JPL's GPS results constitute the main basis for this study, we have also performed an inversion of solutions from six institutions based on four space techniques. The data input for these additional analyses consist of the velocities of:

(1) 509 GPS sites from JPL's solution,

(2), (3) and (4) the 52 VLBI, 20 SLR and 37 DORIS sites employed in Argus *et al.* (2010),

(5) 36 GPS sites in Fennoscandia [BIFROST data from 1994 to 2006, determined by Lidberg *et al.* (2010)] and

(6) 142 GPS sites in the Canadian Base Network (estimated using four campaigns from 1996 to 2011 by M. Craymer electronic communication 2012). The estimated parameters consist of the rotational and translational velocities between the original reference frames of the four space techniques, the angular velocities of the major plates, and the velocities of sites on plates moving significantly due to postglacial rebound or current ice loss. The velocities of sites on plates are deduced from their residuals (Argus & Peltier 2010).

For Antarctica, the focus of this study, we examine 66 estimates of site velocity (Table 1). We determine the velocities of 59 sites from GPS data from 1996 to 2012 (Table 1, Figs S2 and S3, Figs 6–8). We also examine four site velocity estimates from Thomas *et al.* (2011) and three from Groh *et al.* 2012; Table 2). Thirteen of the 59 site velocities that we estimate are weighted means from 2 to 4 monuments located within 5 km of each other. The remaining 43 site velocities are based on data taken at just one monument. The velocity of O'Higgins, for example, is estimated from four monuments, as is the velocity of McMurdo. Maitri's velocity is estimated from three campaign GPS sites. We do not tie the velocity of DORIS sites to that of nearby GPS sites. The 59 uplift rates that we estimate are greater in number than the 35 uplift rates estimated in Thomas *et al.* (2011) that were employed in the deglaciation reconstructions of Whitehouse *et al.* (2012a,b).

2.3 Reference frame

In this study we define the translational velocity of Earth's reference frame using a slightly different assumption than that we have previously employed (Argus *et al.* 2010, 2011; Argus & Peltier 2010). We estimate the velocity of Earth's center by simultaneously minimizing:

(1) differences between observed vertical rates observed with space geodesy and those predicted by ICE-6G_C (VM5a) and

(2) differences between observed horizontal site velocities observed with space geodesy and those predicted by the plate angular velocities fit to the observed horizontal site velocities.

Table 1. Observed velocities and predicted uplift rates.

Place	Lat. °N	Lon. °E	Horizontal Speed mm yr^{-1}	Azim. °	Vertical Up mm yr^{-1}	VM5a mm yr^{-1}	CIL mm yr^{-1}	Technique, site abbreviation observation time period in year
						ICE6G_C		

Place	Lat. °N	Lon. °E	Speed mm yr^{-1}	Azim. °	Up mm yr^{-1}	VM5a mm yr^{-1}	CIL mm yr^{-1}	Technique, site abbreviation observation time period in year
25 East Antarctic sites reflecting primarily postglacial rebound and on the Antarctica Plate							
Heimefrontfjella	−74.58	−11.23	0.8 ± 2.6	172	1.7 ± 5.7	3.2	0.2	G svea 3
Vesleskarvet	−71.67	−2.84	0.4 ± 0.7	−102	1.5 ± 1.5	1.9	0.1	G vesl 13
Maitri	−70.77	11.74	1.0 ± 0.6	116	1.3 ± 1.3	1.2	0.1	G mait 9 for1 13 for2 13 campaign
Marion island	−46.88	37.86	1.8 ± 4.0	−5	−3.3 ± 8.9	−0.3	−0.1	G marn 2
Syowa	−69.01	39.58	0.4 ± 0.7	−97	0.6 ± 1.5	0.9	0.0	G syog 13 V syowa 3
Mawson	−67.60	62.87	0.4 ± 0.5	−119	0.2 ± 1.2	0.6	0.0	G maw1 16
Kerguelen island	−49.35	70.26	0.4 ± 1.0	35	1.1 ± 2.2	−0.5	−0.1	G kerg 9
a351	−72.91	74.91	0.6 ± 3.1	154	1.1 ± 7.0	0.9	0.0	G a351 2
Davis	−68.58	77.97	0.1 ± 0.9	−110	−0.8 ± 2.0	0.2	0.0	G dav1 10
Casey	−66.28	110.52	0.9 ± 0.7	−59	1.7 ± 1.6	1.1	−0.0	G cas1 12
Dumont D'Urville	−66.67	140.00	0.8 ± 0.7	41	−0.2 ± 1.6	0.4	0.0	G dum1 12
Lonewolf Nunatak	−81.35	152.73	0.9 ± 2.3	−107	1.7 ± 5.0	2.1	0.2	G lwn0 4
Westhaven Nunatak	−79.85	154.22	1.0 ± 2.2	−100	3.2 ± 4.9	1.9	0.2	G whn0 4
Butcher Ridge	−79.15	155.89	0.7 ± 1.8	−109	1.6 ± 4.1	1.8	0.2	G buri 4
Iggy Ridge	−83.31	156.25	0.5 ± 2.4	−165	3.3 ± 5.4	2.2	0.2	G iggy 3
Brimstone Peak	−75.80	158.47	0.6 ± 1.9	−152	1.3 ± 4.3	1.9	0.1	G brip 4
Mount Fleming	−77.53	160.27	0.6 ± 1.5	−171	2.7 ± 3.2	2.3	0.1	G flm5 6
Deverall island	−81.48	161.98	0.6 ± 2.3	−131	2.7 ± 5.2	3.8	0.2	G devi 3
Mount Coates	−77.81	162.00	0.4 ± 2.2	−156	2.3 ± 4.9	2.1	0.1	G cote 4
Fishtail Point	−78.93	162.56	0.5 ± 1.5	−178	3.0 ± 3.3	2.5	0.2	G ftp4 6
Cape Roberts	−77.03	163.19	0.5 ± 1.5	175	2.2 ± 3.2	2.0	0.1	G rob4 6
Terra Nova Bay	−74.70	164.10	0.8 ± 0.9	88	−0.4 ± 2.0	1.6	0.1	G tnb1 9
McMurdo	−77.85	166.67	0.2 ± 0.5	104	1.0 ± 1.2	1.6	0.2	G crar 10 sctb 5 mcm4 9 mcmd 6
min0	−78.65	167.16	0.6 ± 2.0	−179	2.7 ± 4.4	2.1	0.2	G min0 4
ramg	−84.34	178.05	0.6 ± 2.3	−167	3.1 ± 5.1	4.0	0.3	G ramg 4
9 Northern Antarctic Peninsula sites rising in elastic response to current ice loss							
O'Higgins	−63.32	−57.90	2.3 ± 0.7	151	5.1 ± 1.4	1.4	4.8	V ohiggins 11 G ohi2 7 ohi3 7 ohig 7
Palmer	−64.78	−64.05	1.8 ± 0.8	−117	7.5 ± 1.7	2.3	3.1	G palm 11
Duthers Point	−64.80	−62.82	2.4 ± 2.2	−114	12.4 ± 5.0	2.7	6.2	G dupt 4
Robertson island	−65.25	−59.44	5.3 ± 2.8	166	8.7 ± 6.3	2.4	3.1	G robi 3
Hugo island	−64.96	−65.67	1.1 ± 3.2	155	1.7 ± 7.2	1.7	2.0	G hugo 2
Vernadsky	−65.25	−64.25	1.7 ± 2.2	−152	5.2 ± 5.0	2.7	3.3	G vnad 4
Foyn Point	−65.25	−61.65	5.7 ± 3.1	171	14.8 ± 6.8	3.2	6.8	G fonp 3
Cape Framnes	−66.01	−60.56	3.3 ± 3.8	28	15.0 ± 8.4	3.3	4.3	G capf 2
Rothera	−67.57	−68.13	1.2 ± 1.2	158	5.4 ± 2.7	2.1	1.2	G roth 3 rotb 6
17 West Antarctic sites reflecting primarily postglacial rebound							
Mount Howe	−87.42	−149.43	0.8 ± 1.1	61	0.9 ± 2.4	0.6	0.3	G w01a–howe 10 w01b 4
Pescora Escarpment	−85.61	−68.56	0.8 ± 1.7	122	−1.2 ± 3.8	0.5	0.4	G w02a–pece 6 w02b 4
Whichaway Nunataks	−81.58	−28.40	1.6 ± 2.2	141	−1.1 ± 4.7	0.4	0.3	G w03a 4 w03b 4
Cordiner Peaks	−82.86	−53.20	1.9 ± 1.2	153	2.8 ± 2.6	4.2	0.4	G w04b–crdi 9 w04a 3
Wilson Nunataks	−80.04	−80.56	1.2 ± 2.1	−90	5.3 ± 4.7	4.8	0.9	G wiln 3 w05b 3 w05a 3
Mount Johns	−79.63	−91.28	2.8 ± 4.0	−29	−4.7 ± 8.8	−0.6	1.3	G w06a 3
Patriot Hills	−80.32	−81.43	0.8 ± 2.8	−125	4.6 ± 6.2	3.7	0.8	G w07a 3 w07b 3
Mount Sugg	−75.28	−72.18	1.1 ± 1.7	−130	5.0 ± 3.7	6.6	0.8	G w08b–sugg 6 w08a 3
Whtimore Mountains	−82.68	−104.39	1.6 ± 2.0	−11	4.2 ± 3.9	4.5	0.7	G w09b–whtm 6 w09a 3
Mount Paterson	−78.03	−155.02	0.7 ± 1.4	43	5.5 ± 3.1	4.5	0.4	G w12a–patn 8
Howard Nunataks	−77.53	−86.77	1.2 ± 1.9	−54	4.8 ± 4.2	3.4	1.8	G w14a–hown 6
Haag Nunatak	−77.04	−78.29	1.2 ± 1.9	−64	8.0 ± 4.3	7.7	1.1	G w15a–haag 6
Fossil Bluff	−71.31	−68.32	1.4 ± 1.0	−93	2.9 ± 2.3	4.0	0.7	G fos1 9 campaign
Brennecke Nunataks	−72.67	−63.03	0.7 ± 2.5	60	2.1 ± 7.4	4.6	0.6	G bren 3 campaign
Belg	−77.87	−34.63	1.1 ± 1.8	167	0.8 ± 4.8	3.4	0.3	G belg 5
Mount Sidley	−77.14	−125.97	2.5 ± 2.8	81	0.8 ± 6.3	2.6	1.3	G sdly 3
Clark Mountains	−77.34	−141.87	0.9 ± 2.8	79	5.4 ± 6.1	3.0	0.6	G clrk 3
1 South Shetland Plate site							
Frei	−62.19	−58.98	7.1 ± 1.3	−39	−2.9 ± 2.8	1.1	0.9	G frei 7

Table 1.   (*Continued.*)

						ICE6G_C			
Place	Lat. °N	Lon. °E	Horizontal Speed mm yr^{-1}	Azim. °	Vertical Up mm yr^{-1}	VM5a mm yr^{-1}	CIL mm yr^{-1}	Technique, site abbreviation observation time period in year	
7 Sites on Mount Erebus suspected be influenced by volcanic activity									
Hoopers Shoulder	−77.53	166.93	1.8 + 1.3	94	−0.4 + 2.8	1.4	0.2	G hooz 7	
E1	−77.53	167.14	1.2 + 1.0	29	−3.2 + 2.2	1.3	0.2	G e1g2 8	
Rayg	−77.53	167.17	1.0 + 3.0	−49	−8.8 + 6.6	1.3	0.2	G rayg 3	
Truncated Cones	−77.53	167.09	3.5 + 1.0	72	−0.3 + 2.2	1.3	0.2	G cong 9	
Lower Erebus Hut	−77.51	167.14	3.7 + 1.0	171	−1.6 + 2.3	1.3	0.2	G lehg 8	
Nausea Knob	−77.52	167.15	3.8 + 1.1	172	−4.1 + 2.5	1.3	0.2	G naus 7	
Macintosh	−77.53	167.25	3.5 + 2.4	−78	−0.6 + 5.4	1.3	0.2	G macz 3	

Notes: The horizontal velocity is described by a speed (in mm yr^{-1}) and an azimuth (in degrees clockwise of north). Values after the ± are 1-D 95% confidence limits. The right-hand side column list the sites used to estimate the velocity of the place: the space technique (G,GPS; V, VLBI), the site abbreviation, and the effective time period of observation (in year). For example, O'Higgins has 11 yr of VLBI data at site ohiggins, 7 yr of GPS data at three different sites (ohi2, ohi3 and ohig). The velocity of Howe is estimated from 4 yr of campaign data at w01b and 10 yr of campaign and permanent GPS data at the mark in common between w01a and howe. Eight sites have campaign and permanent data at a monument (e.g. w14a–hown). ICE-6G_C (VM5a) is this postglacial rebound model that we present in this study. CIL is the elastic model of current ice loss near Pine Island Bay and Larsen B ice shelf constructed in this study on the basis of GRACE data (CSR Release 5) from 2003 January to 2013 February. The effective time period of observations is defined to be the rms of the time period before an offset and the time period after the offset and the rms of the time period of two or more sites at the same place. We take the standard error in uplift to be 10 mm divided by the effective time period of observation (see Argus *et al.* 2010; Argus & Peltier 2010). We take the standard error in the east and north components of velocity to be 4.5 mm divided by the effective time period of observation. Uncertainties in campaign GPS site velocities are assumed to be 33 per cent larger than uncertainties in continuous GPS site velocities.

In this minimization we employ only sites on plate interiors that are neither beneath nor near areas of postglacial rebound or current ice loss, and we simultaneously estimate the angular velocity of the plates and the velocity of Earth's centre. We have altered our prior assumption because it is now believed that the majority of Earth's surface not near current or past areas of loss of grounded ice are moving very slowly in the vertical. Rotational feedback associated with the wander of Earth's spin axis towards Canada is now agreed (Chambers *et al.* 2010, 2012; Peltier *et al.* 2012) to generate a degree-2, order-1 (spherical harmonic) deformation such that the extrema of the quadrapolar pattern on Earth's surface that characterizes this influence are either rising or falling only as fast as 0.4–0.7 mm yr^{-1}. We have used this knowledge to strongly constrain Earth's reference frame. Thus, the velocity of Earth's centre that we estimate depends only weakly on the postglacial rebound that is corrected for. The estimate determined by assuming ICE-6G_C (VM5a) differs by just 0.2 mm yr^{-1} from the estimate determined assuming the postglacial rebound model of A *et al.* (2013) (Fig. S4). This is because the vertical predictions of the two models differ by less than 0.5 mm yr^{-1} in the areas away from the ice sheets that we have used to define the reference frame. The model of A *et al.* (2013) is based on the same deglaciation history and viscosity model as the ICE-5G (VM2) model of Peltier (2004).

We estimate the velocity of Earth's centre relative to the velocity of CM in ITRF2008 (Altamimi *et al.* 2011) to be: X − 0.18, Y 0.13, Z −0.56 mm yr^{-1} (Fig. S4). X and Y are nearly zero; Z is about 1.5 mm yr^{-1}. At high northern latitudes in Canada and Scandinavia our reference frame yields 0.5 mm yr^{-1} less uplift than ITRF2008. At high southern latitudes in Antarctica our reference frame yields 0.5 mm yr^{-1} more uplift than ITRF2008. (The Z component of 0.56 mm yr^{-1} multiplied by sin(60°N) equals 0.48 mm yr^{-1}).

Minimizing vertical differences from a postglacial rebound model constrains the reference frame more strongly than minimizing the horizontal differences from rigid plates. This is evident in that the joint determination of the velocity of CM (Z 0.56 mm yr^{-1}) is one-quarter of the way from the verti-

cal determination (0.39 mm yr^{-1}) to the horizontal determination (Z 1.04 mm yr^{-1}; Fig. S4, see the light blue ellipses in b, c and d).

The velocity of CM in ITRF2008 has long been the standard used to define the velocity of Earth's centre. The time-series for CM suggests, however, that this velocity is not constrained very tightly. For example, the estimate of the Z component of the velocity of CM from 1993 to 2000 differs from the estimate from 2001 to 2008 by 1.15 mm yr^{-1} (Argus 2012). Using spectral analysis and data decimation, Argus (2012) estimated the uncertainty in the velocity of CM to be ±0.4 mm yr^{-1} in X, ±0.4 mm yr^{-1} in Y and ±0.9 mm yr^{-1} in Z (1-D 95% confidence limits.) Thus, the velocity of CM from SLR is quite uncertain in Z.

Thomas *et al.* (2011) define Earth's reference frame using the velocity of CM in ITRF2008. Our new estimate of the velocity of Earth's centre yields 0.5 mm yr^{-1} more uplift in Antarctic than theirs. This difference is significant for the 10 GPS sites along the Antarctic coast with 8–15 yr of permanent GPS data.

Argus *et al.* (2011) defined the reference frame by minimizing the horizontal differences. This determination is slightly tenuous in that postglacial rebound may be deforming the plates in the horizontal, violating the assumption of plate rigidity in the determination. Tregoning *et al.* (2013) suggest that postseismic transients of the M_9 2004 Sumatra, 2010 Chile and 2011 Japan earthquakes might also cause the plate interiors to deform. Our new estimate of the velocity of Earth's centre yields 0.5 mm yr^{-1} less uplift in Antarctica than in Argus *et al.* (2011).

Argus *et al.* (2007, 2012) argue that their determinations of the velocity of Earth's centre (labelled CE in Fig. S4) represents an estimate of the velocity of CM. The argument for the vertical determination is straightforward. Removing the predictions of a postglacial rebound model from the vertical observations yields an estimate of the velocity of CE because that is the reference frame in which the postglacial rebound predictions are determined. The present velocity of CM relative to CE due to postglacial rebound is negligible because ice has not been lost in the postglacial rebound models since 4 ka. Current ice loss results in a significant velocity of CM relative to CE. This velocity would be 0.22 mm yr^{-1} if Greenland were
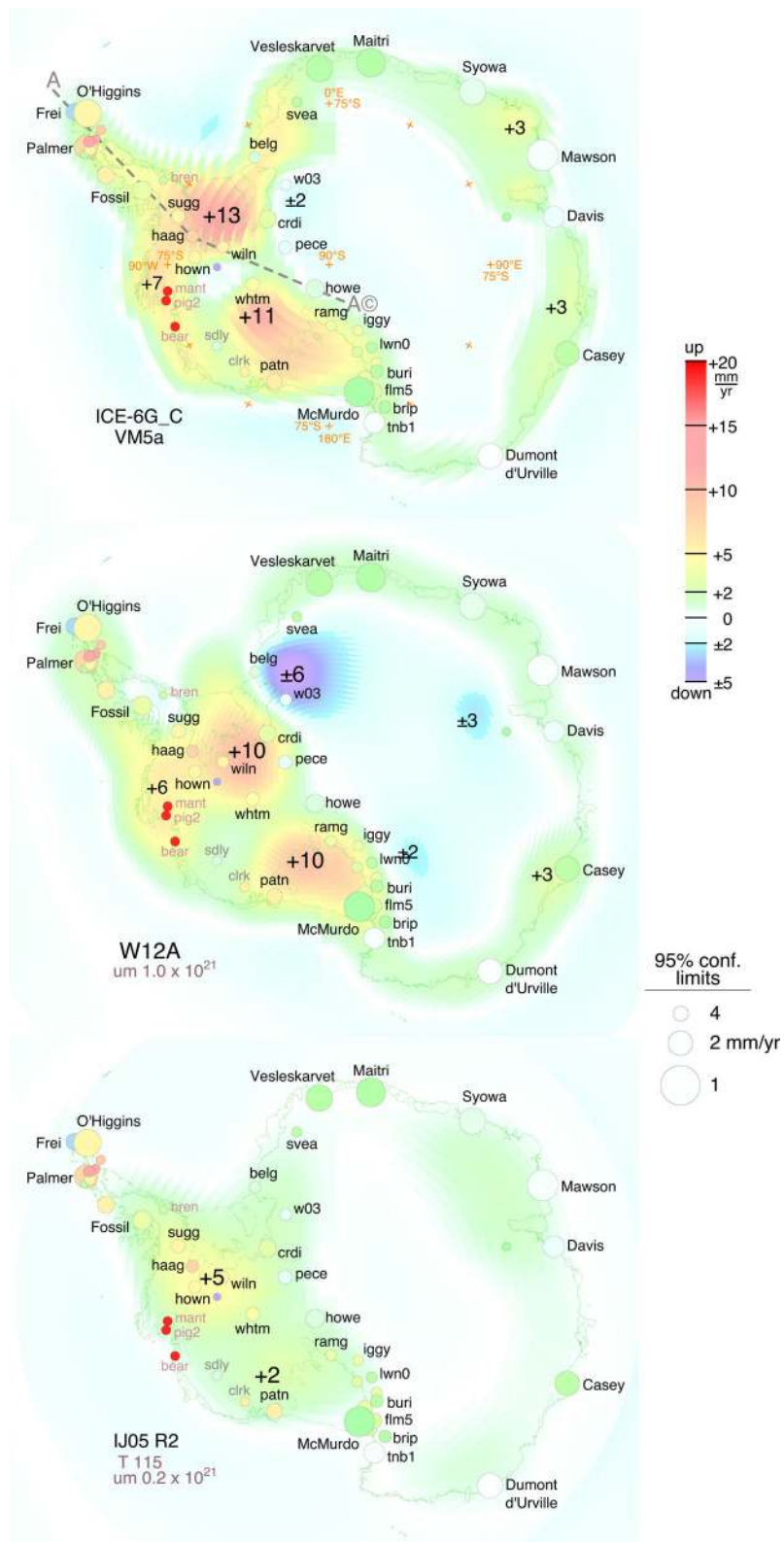
Figure 6. Estimates of uplift at GPS sites (circles) are compared with the predictions of postglacial rebound models (top) ICE 6G C (VM5a), (middle) W12A (Whitehouse *et al.* 2012b), and (bottom) IJ05 R2 (Ivins *et al.* 2013). The colours of the circles indicate the vertical rate of motion estimated by GPS as shown by the legend. The larger the circle the more certain is the estimate. Mawson, the most tightly constrained uplift rate, has an uncertainty of ± 1.2 mm yr^{-1} (95% confidence limits). Sugg, a site with campaign WAGN data connected to continuous ANET data, has an uncertainty of ± 3.7 mm yr^{-1}.
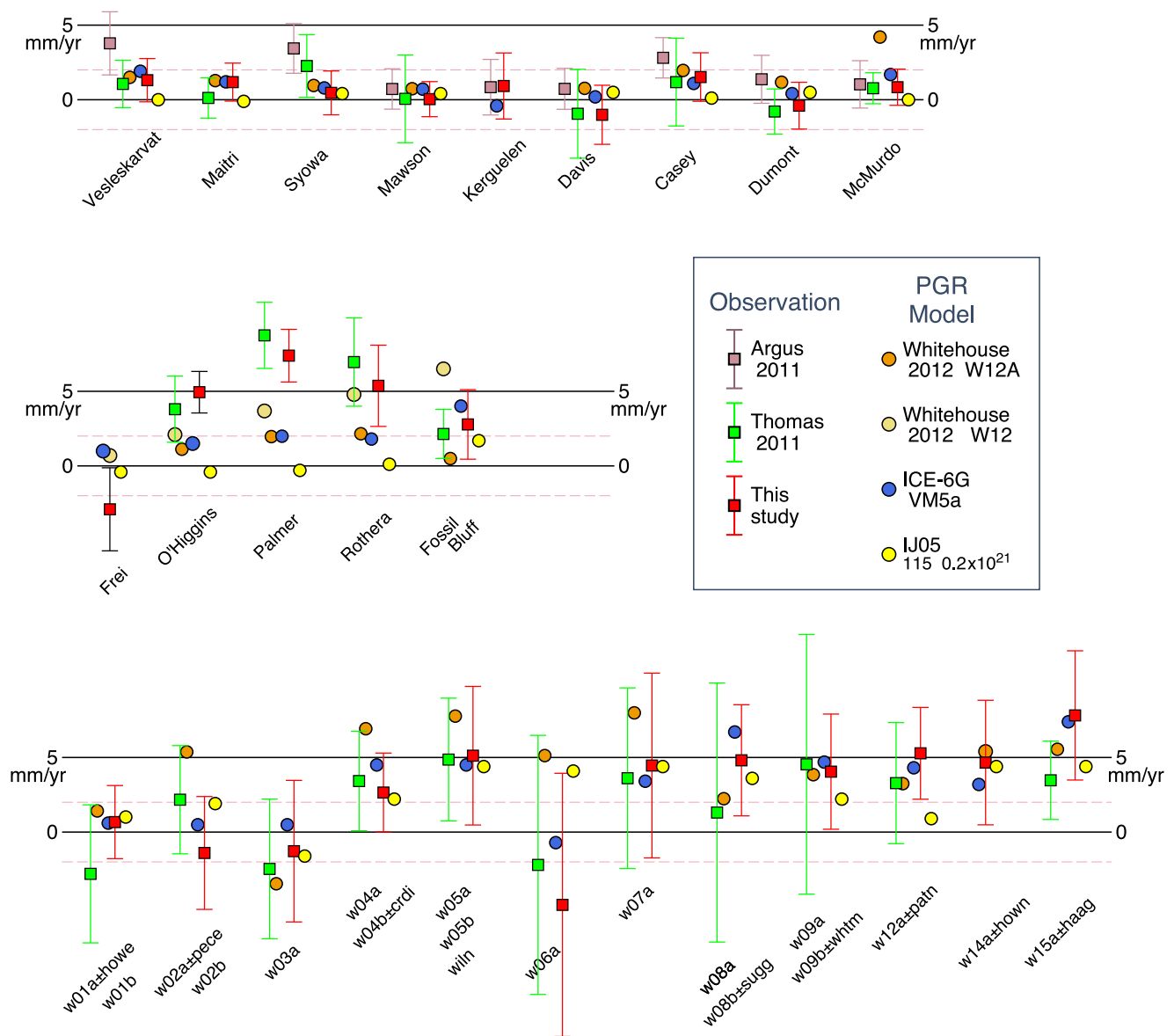
Figure 7. GPS observations of uplift are compared with predictions of postglacial rebound models (top) in East Antarctica, (middle) on the Antarctic Peninsula, and (bottom) in the interior of West Antarctica. The W12 and W12A models are nearly equal in East Antarctica and the West Antarctic interior and differ on the Antarctica Peninsula. Error bars are 95 per cent confidence limits. Standard errors in uplift are taken to be, for permanent GPS sites, 10 mm divided by the effective time period of observation; and, for campaign GPS sites, 13.3 mm divided by the effective observation time. The error bars of the Thomas observations are not their estimates but rather estimated by us using our methods. This study's estimate of uplift of Sugg is 5 $\pm$3 mm yr^{-1}, a (marginally) significant 4 mm yr^{-1} faster than that in Thomas *et al.* (2011). This study's estimate of uplift of Haag is 8 $\pm$ 3 mm yr^{-1}, a (marginally) significant 4 mm yr^{-1} faster than Thomas' estimate. McMurdo is rising at 1 $\pm$1 mm yr^{-1}, a significant 3.5 slower than predicted by the postglacial rebound model of Whitehouse *et al.* (2012b). Most velocities in the west Antarctic interior are the mean of 1 velocity coming from a campaign site (e.g. w01b) plus a campaign site connected to a permanent site (w01–howe).

losing ice at 200 Gt yr^{-1} and there were no ice loss elsewhere (Argus 2007, 2012; Métivier *et al.* 2010; Shepherd *et al.* 2012). The estimate of the velocity of Earth's centre determined in this study lies within the 95% confidence limits of the velocity of CM from SLR.

2.4 Rotational feedback

The ICE-6G_C (VM5a) model consists of two components, an ice sheet component and a rotational feedback component (*cf.* Argus & Peltier 2010, fig. 3). The ice sheet component is the solid Earth's viscoelastic response to unloading of the former ice sheets and the

resulting loading of the ocean basins by water (surface mass loads). The rotational feedback component is the solid Earth's viscoelastic response to secular polar wander (centrifugal body force), which also ultimately results from ice loss.

The secular polar wander predicted by ICE-6G_C (VM5a) is consistent with the observed mean velocity of the North Pole of Earth's spin axis over the past 100 yr at 0.0035 arcsec yr^{-1} along the 75°W meridian (Gross & Vondrak 1999; Argus & Gross 2004). Rotational feedback generates a degree-2, order-1 deformation of the solid Earth. Uplift and subsidence are a maximum of 0.7 mm yr^{-1} at four places along the 75°W–105°E great circle, two at 45°N and two at 45°S. Rotational feedback also causes places to move horizontally
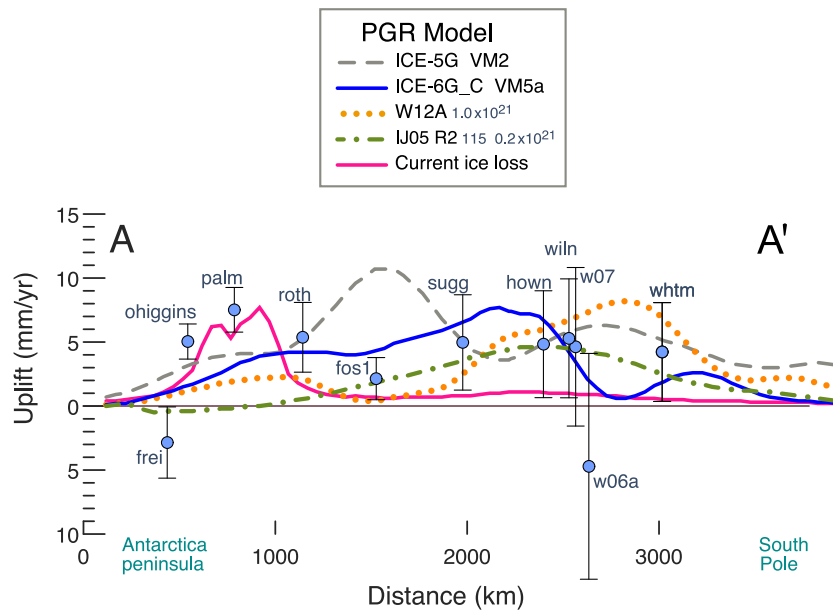
Figure 8. Uplift rate along profile A′–A′. Error bars are 95% confidence limits. The location of profile A–A′ is shown in Fig. 6.

Table 2. Observed uplift rates from other studies.

			ICE6G_C			
	Lat.	Lon.	Vertical Up	VM5a	CIL	Technique, site abbreviation observation time
Place	°N	°N	mm yr⁻¹	mm yr⁻¹	mm yr⁻¹	in year
			From Thomas *et al.* (2011)			
smrt	−68.12	−67.10	−0.2 ± 6.4	3.1	1.2	G smrt 3
a368	−74.29	66.79	0.4 ± 4.4	2.4	0.0	G a368 6 campaign
aboa	−73.04	−13.41	1.4 ± 2.8	3.2	0.2	G aboa 7
Fossil Bluff	−71.31	−68.32	2.1 ± 1.6	4.0	0.7	G fos1 6
			From Groh *et al.* (2012)			
mant	−74.78	−99.37	30.0 ± 6.5	5.9	23.2	G mant 4 campaign
bear	−74.57	−111.89	28.1 ± 6.5	5.0	19.4	G bear 4 campaign
pig2	−74.51	−102.44	17.9 ± 6.5	5.7	11.5	G pig2 4 campaign

Notes: See caption of Table 1. Uncertainties are not from the original studies. We estimated the uncertainty in the uplift rate from the effective time period of observations as described in Table 1.

away from the areas of subsidence and towards the area of uplift. This sense is opposite that for postglacial rebound because the solid Earth's response to a body force (rotational feedback) differs from that to a surface load (postglacial rebound). The horizontal speed is maximum at four places along the 75°W–105°E great circle, two along the Equator and two at the North and South poles (Argus & Peltier 2010, fig. 3).

In Antarctica vertical motion due to rotational feedback is predicted to vary. The vertical predictions along the 75°W–105°E great circle change gradually from 0.6 mm yr⁻¹ in the Northern Antarctic Peninsula (near O'Higgins), to zero at the South Pole, to −0.5 mm yr⁻¹ along the Wilkes Land coast (near Casey). The vertical predictions along the 15°E–165°W great circle are nearly zero.

In Antarctica horizontal motion due to rotational feedback is predicted to be everywhere about 0.5 mm yr⁻¹ parallel to the 75°W–105°E great circle towards South America (bottom of Fig. S5). This contribution to horizontal motion can be absorbed into the definition of the Antarctica plate by adjusting the angular velocity of the plate, as we discuss below.

3 MAIN GPS RESULTS

3.1 Vertical motion of the Antarctic coast

GPS tightly constrains the rate of uplift of 10 sites along the Antarctic coast (Figs 6 and 7 and Fig. S2). Each site has 10–18 yr of continuous GPS data, allowing the uplift rate to be determined accurately.

Uplift along the East Antarctica coast ranges from −1 mm yr⁻¹ to 1.5 mm yr⁻¹. At four sites our new estimates of uplift are 1.5–3 mm yr⁻¹ slower than those we estimated 3 yr ago (Argus *et al.* 2011). Just 0.5 mm yr⁻¹ of the difference is due to the difference in reference frame between this study and Argus *et al.* (2011). The difference is due mainly to the improvement in the GPS solution and to different offsets being estimated. At Syowa we estimate an offset at a different time than previously. At Vesleskarvet we no longer estimate an offset. At Casey we now introduce an offset. At Davis, the evolution of the north component now requires two offsets. At Dumont, the series simply yields a slower uplift rate. Although our estimates of uplift rate depend somewhat on whether or not offsets

are estimated (see also Gazeaux *et al.* 2013), our new position series (Fig. S2) are better fit by linear least squares regression then were our old series (Argus *et al.* 2011, fig. S1). This further increases confidence in the quality of our new estimates.

Our revised estimates of the 10 most tightly constrained uplift rates are within 1 mm yr⁻¹ of those estimated previously by Thomas *et al.* (2011), with the exception of a 2 mm yr⁻¹ difference at Syowa. Furthermore, at Mawson we have no offsets over the 17 yr of observations, fewer than the two offsets posited in the analysis of Thomas *et al.* (2011).

3.2 Uplift of the West Antarctica interior

The velocities of eight campaign GPS sites in the interior of West Antarctica were estimated by Bevis *et al.* (2009), Argus *et al.* (2011) and Thomas *et al.* (2011) by connecting summer GPS campaigns over 5 yr to 1 month of succeeding permanent GPS observations at the same marks. The campaign data are from the West Antarctica GPS Network (WAGN). The permanent GPS data are from the Antarctica segment of the (POLENET) Polar Earth Ob-

serving Network [www.polenet.org]. In this study we connect the WAGN campaign data to 3–5 yr of permanent GPS data, thus markedly improving the velocity estimates (Fig. S3.)

3.3 Horizontal oscillations in the West Antarctic interior

Sites in the interior of West Antarctica are moving back and forth horizontally with the season, attaining their maximum lateral position in one direction in the summer (February), and in the opposite direction in the winter (August). Seven sites show peak-to-peak amplitudes ranging from 9 to 33 mm (Figs 9 and 10). These large horizontal annual oscillations complicate the fitting of a velocity to sites with both sparse campaign and permanent GPS position estimates. This is because estimates of position spaced closely in time are strongly correlated, and daily estimates of position during the time of continuous observation are thus weighted too heavily relative to campaign estimates. We have overcome this difficulty in straightforward fashion by eliminating all data during the time of continuous observation except those taken on either the 1st or the 16th of the month (Fig. 9). This method results in a reasonable
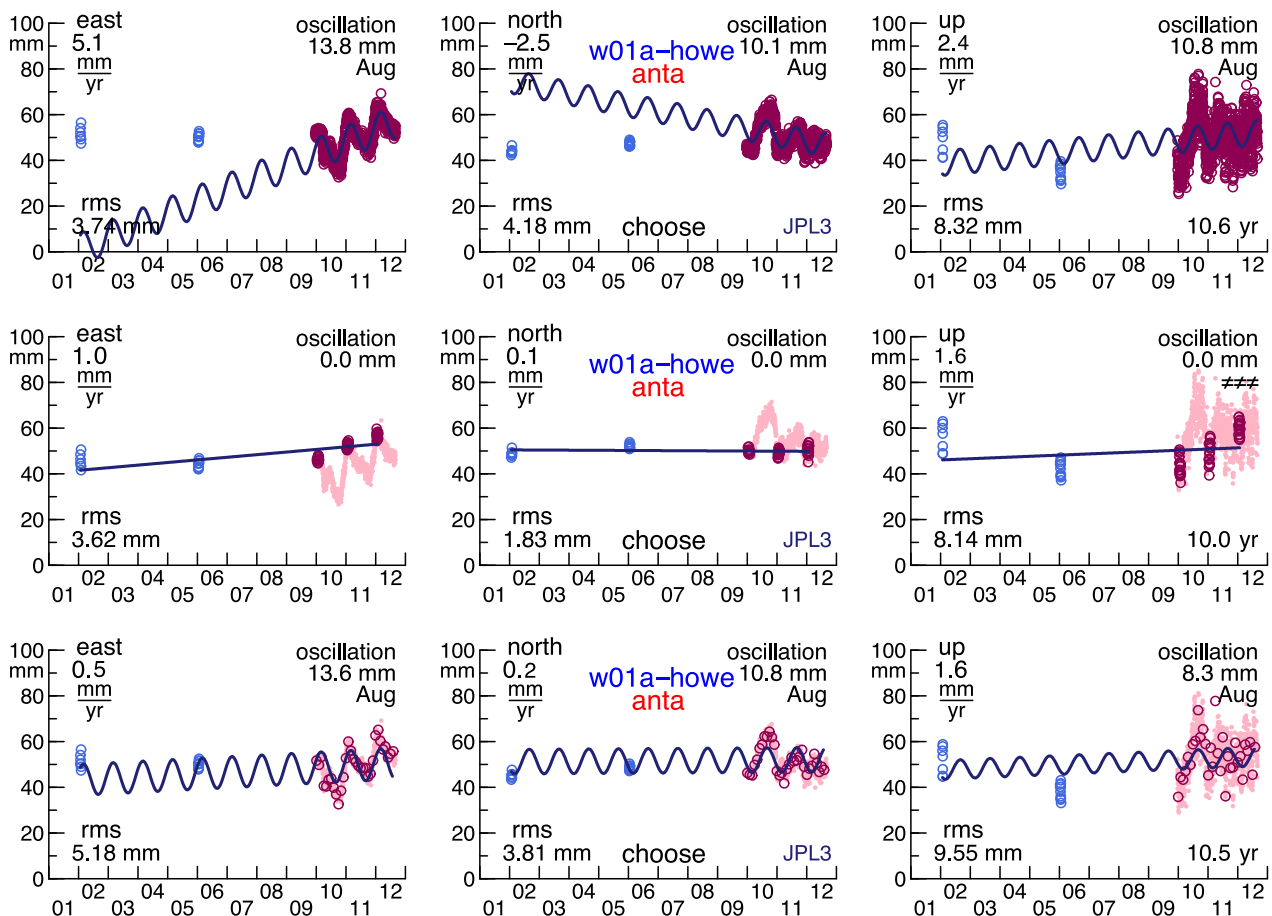
Figure 9. Three methods to fit the campaign WAGN and permanent ANET data. The east component is plotted in the left-hand side column, the north component in the centre column, and the up component in the right-hand side column. (blue circles) campaign data, (red circles) inverted permanent data, (small pink dots) omitted permanent data. (Top row) If all position estimates are given equal weight and fit with a velocity and a sinusoid, then the estimated velocity poorly fits the campaign data. This is because successive estimates of position are strongly correlated, resulting in too much weight being given to the daily permanent data relative to the yearly campaign data. (Middle row) If only permanent data taken on the days of the year of campaign observations are fit with a velocity without a sinusoid, then the estimated velocity fits the data well, but the seasonal oscillation is not estimated. (Bottom row) If only permanent data taken on the 1st or 16th day of the month are inverted and fit with a velocity and a sinusoid, then the estimated velocity and estimated oscillation fits the data well. Given is (at top left) the best-fitting rate, (top right) the peak-to-peak oscillation and time of maximum vertical position, (bottom left) rms misfit, and (bottom right) effective time period of observation.
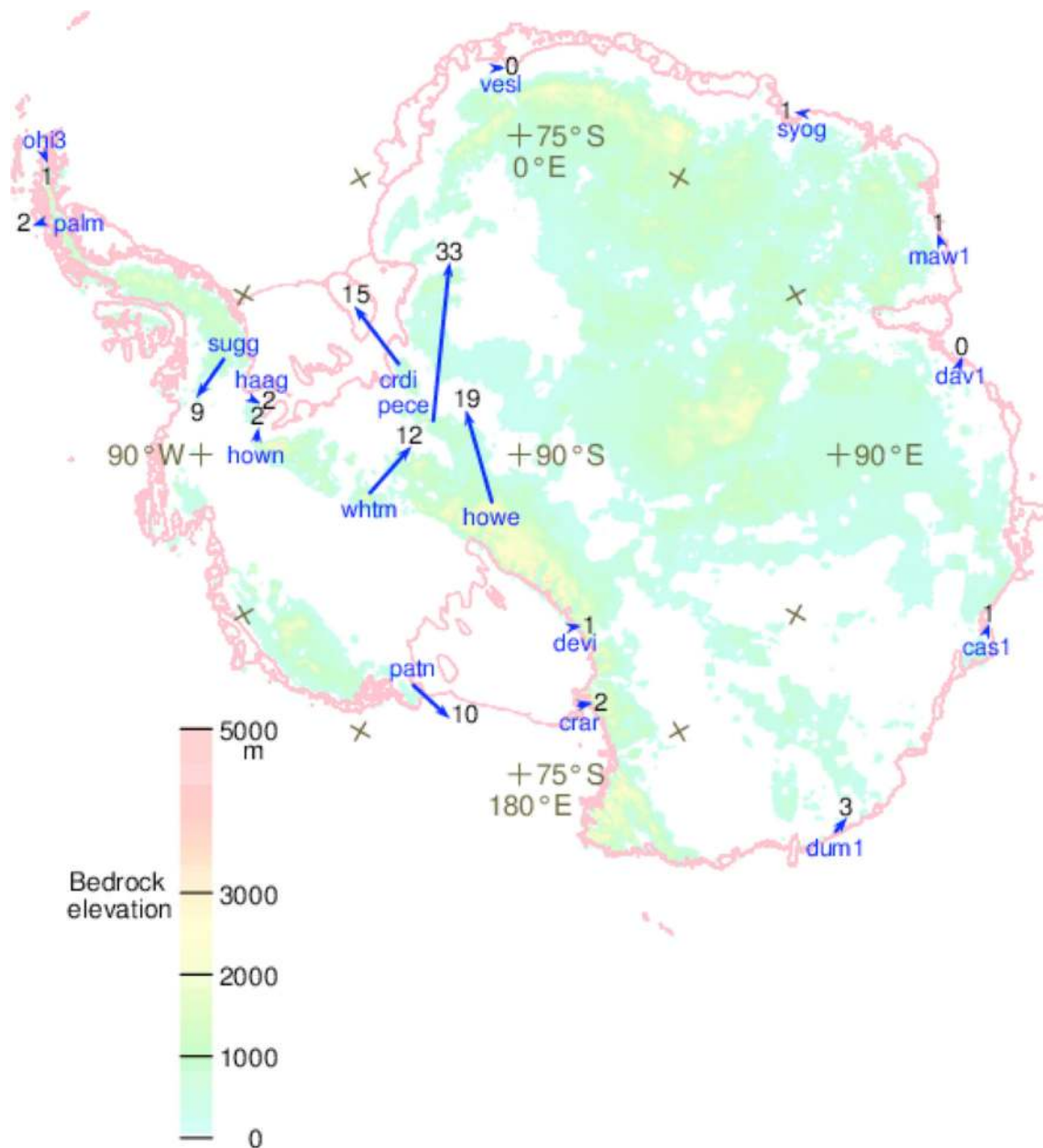
Figure 10. Seasonal horizontal motion of sites from the winter (August) to the summer (February). This seasonal horizontal motion (given in millimetre) is calculated from the sinusoid fit to series of the east and north components of position.

fit of the campaign and permanent GPS data at all eight sites with connections between campaign and permanent GPS sites (Fig. S3).

Possible causes of this large horizontal oscillation include:

(1) snow and ice accumulating on and near the GPS antennae that slow the GPS signal, or that cause the GPS signal to take different paths to the antenna,

(2) tilting of the GPS structure on its square base, perhaps by shortening and lengthening of 1 of 4 screws beneath the base,

(3) heating and cooling of the bedrock in the 1 or 2 m beneath the GPS structure,

(4) true movement of the deep bedrock beneath the GPS structure.

We doubt the cause to be (4) since mass loading would cause more vertical than horizontal movement. Typical values of the thermal expansion coefficient of rock also suffice to rule out (3).

(An $8 \times 10^{-6}\,^\circ\text{C}^{-1}$ linear coefficient of thermal expansion times 2 m depth times a 30 °C seasonal temperature variation delivers an estimate of motion of just 0.5 mm.) Furthermore, the cause cannot be due to (2) because other GPS sites having an identical GPS structure do not exhibit horizontal oscillations. We therefore suspect the true cause of the observed oscillations to be (1) (Larson & Nievinski 2012; Larson 2013).

3.4 Horizontal Velocities in Antarctica

3.4.1 Definition of Antarctica Plate

We define the Antarctic Plate and estimate its angular velocity following the methods of Argus *et al.* (2010) and Argus & Peltier (2010). A standard model is first constructed in
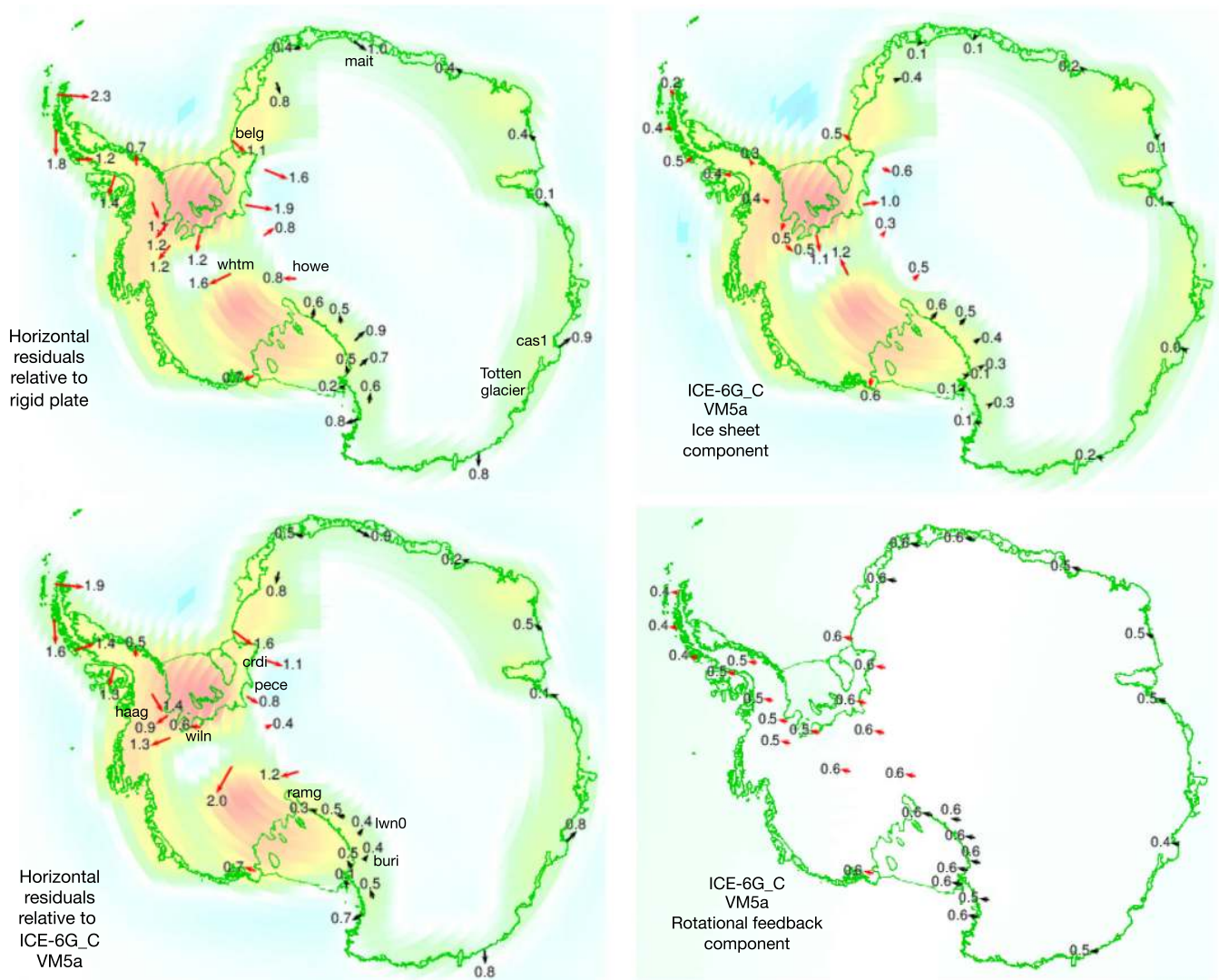
Figure 11. Analysis of horizontal site velocities. Residual horizontal velocities relative to the rigid plate model (top left) are compared with (horizontal site velocities relative to ICE-6G_C (VM5a; bottom left). The ICE-6G_C horizontal predictions consist of an ice sheet component (top left) and a rotational feedback component (bottom right). Sites in East Antarctica used to define the Antarctic Plate (black vectors) are distinguished from sites in West Antarctica and on the Antarctica Peninsula that are not (red vectors). Speeds are given in millimetres per year. Sites with poorly constrained horizontal velocities are omitted.

which Earth's major plates are rigid horizontally and deform vertically as predicted by ICE-6G_C (VM5a). The translational velocity of Earth's reference frame and the angular velocities of the major plates are next estimated by minimizing the sum of squares of differences between this model and the observed 3-D site velocities.

Twenty-three sites in East Antarctica and two sites on Kerguelen island and Marion island are assumed to be on the Antarctica Plate and used to estimate the angular velocity of the plate. The data most tightly constraining the angular velocity come from Kerguelen island and eight sites along the East Antarctic coast (Veleskarvet, Maitri, Syowa, Mawson, Davis, Casey, Dumont d'Urville and McMurdo). In the horizontal, East Antarctic and the two islands are nearly a rigid plate (Fig. 11, top left). The weighted rms (wrms) residual speed of the 25 site velocities is $0.62\,\mathrm{mm\,yr^{-1}}$, comparable to the 0.5–$1.1\,\mathrm{mm\,yr^{-1}}$ wrms residual speed for the other major plates (Argus *et al.* 2010). Two of the 25 sites have residual horizontal site velocities that are significant with 95% confidence. Maitri is

estimated to have a residual velocity of $1.1 \pm 0.6\,\mathrm{mm\,yr^{-1}}$ towards southeast (1-D 95% confidence limits) due to an unknown reason, although the uncertainty in the velocity may be underestimated because the GPS data are from campaigns. Casey is estimated to be moving northwest at $0.9 \pm 0.7\,\mathrm{mm\,yr^{-1}}$, likely in elastic response to current ice loss at Totten glacier to its southeast.

3.4.2 Northern Antarctica Peninsula

As in Argus *et al.* (2010, 2011), we find O'Higgins to be moving southeast at a significant $2.3 \pm 0.7\,\mathrm{mm\,yr^{-1}}$ relative to the Antarctic Plate (Fig. 11, top left). O'Higgins is located along the northern coast of the peninsula. Current ice loss from the peninsula would cause O'Higgins to move north in elastic response to unloading, in the direction opposite to that observed. The Shetland islands are north of the Northern Antarctic Peninsula. Current ice loss from the Shetland islands could cause O'Higgins to move south in elastic

response, but the ice loss there is too small to cause O'Higgins to move significantly. We conclude that the cause of O'Higgins significant velocity relative to the Antarctic Plate remains unknown. Other sites in the Northern Antarctic Peninsula are suspected or known to be moving in elastic response to current ice loss near the former Larsen B Ice Shelf.

3.4.3 *Outward horizontal motion in viscous response to early Holocene unloading of ice at Ronne and Ross Ice Shelves*

Sites along the southern margin of Ronne–Filchner Ice Shelf are observed to be moving horizontally away from the ice shelf at 0.8–1.2 mm yr^{-1} (Fig. 11, top left). The present location of Ronne–Filchner Ice Shelf corresponds to a local maximum in ice loss since the Last Glacial Maximum in ICE-6G_C. Therefore, this horizontal motion is inferred to be due to Earth's viscous response to unloading of early Holocene ice there.

Sites along the southern margin of Ross Ice Shelf are similarly observed to be moving away from the ice shelf at 0.5–0.9 mm yr^{-1}. In ICE-6G_C, the western Ross Ice Shelf corresponds to a local maximum in Holocene ice loss. The horizontal motion is again inferred to be due to the postglacial rebound process.

3.4.4 *The fit of ICE-6G_C (VM5a) to the horizontal data*

Evaluating the fit of ICE-6G_C (VM5a) to the horizontal data is complicated by the rotational feedback component of the model. The ice sheet component of ICE-6G_C (VM5a) predicts there to be slow horizontal motion away from the Ronne–Filchner Ice Shelf at 0.5–1.1 mm yr^{-1} and slow horizontal motion away from the Ross Ice Shelf at 0.3–0.6 mm yr^{-1} (Fig. 11, top right), in agreement with the observed outward horizontal motion (Fig. 11, top left). The rotational feedback component of ICE-6G_C (VM5a; Fig. 11, bottom right), however, predicts all of Antarctic to be moving at about 0.6 mm yr^{-1} parallel to the 75°W–105°E great circle towards South America. This coherent motion of Antarctica can nevertheless be readily incorporated by adjusting the estimate of the angular velocity of the Antarctic Plate by a rotation of 0.005° Myr^{-1} about a pole at 0°N 15E. Thus, the complete horizontal predictions (Fig. S5, left-hand side) agrees well with the horizontal observations in the ICE-6G_C (VM5a) reference frame (Fig. S5, right-hand side).

ICE-6G_C (VM5a) fits the horizontal data slightly better than the rigid plate model, but insignificantly so. Correcting for the predictions of the postglacial rebound model reduces the wrms residual speed of the 42 horizontal site velocities from 0.79 mm yr^{-1} (Fig. 11, top left) to 0.73 mm yr^{-1} (Fig 11, bottom left). Chi-square decreases from 102.0 to 91.4; an *F*-test indicates this reduction to be insignificant ($p = 0.25$). Residuals of four sites along the Ross Sea coast are reduced (Ramg, Lwn0, Buri and Whn0,). Residuals of four sites near the Weddell Sea are also reduced (Haag, Wiln, Crdi, Pece), but the residuals of three sites there are enlarged (Belg, Whtm, Howe).

The wrms residual speed of ICE-6G_C (VM5a) is just 0.73 mm yr^{-1}, comparable to that of the other major plates (Argus *et al.* 2010). (The fastest estimated face-value residual speeds are for the sites with the least data and largest uncertainties.) Given this misfit, and that the horizontal residuals relative to the postglacial rebound model exhibit no systematic pattern, we conclude that the ICE-6G_C (VM5a) fits the horizontal data well with there being no need for lateral variation in mantle viscosity.

4 MODELS OF POSTGLACIAL REBOUND

4.1 ICE-6G_C (VM5a)

The individual members of the University of Toronto series of postglacial rebound models have been constrained primarily by Holocene RSL histories determined by radiocarbon dating of beach terraces and other sea level index points (see Peltier *et al.* 2002 for the methods used to characterize such constraints on RSL history). The models account for the exchange of mass between grounded ice on the continents and water in the ocean basins as well as the effect of the changing surface mass load on both the solid Earth and the distribution of meltwater throughout the oceans. The ICE-6G_C (VM5a) model is, as was its predecessor ICE-5G (VM2), fit to hundreds of such RSL histories. Raised beach terraces along the coasts of the previously ice-covered regions of North America and Europe tightly constrain, respectively, the models of Laurentian and Fennoscandian rebound. The coral-based RSL record from the island of Barbados and similar records from other oceanic islands provide strong constraints upon the total loss of grounded continental ice that has occurred since Last Glacial Maximum. ICE-6G_C (VM5a) differs from ICE-5G (VM2) in three primary respects. First, ICE-6G_C (VM5a) is fit to GPS uplift rates tightly constraining postglacial rebound in the interior of Canada (Argus & Peltier 2010; Peltier *et al.* 2014), including results from GPS campaign sites in the Canadian Base Network (Craymer *et al.* 2011). The new model therefore corrects the misfits identified in Argus & Peltier (2010) for sites in Canada. At Last Glacial Maximum the ice sheet thickness in ICE-6G_C (VM5a) is, relative to ICE 5G (VM2), required to be thicker in Quebec, thinner in Manitoba, thinner near Yellowknife (Northwest Territories) and thicker near the Northern Alberta–British Columbia border. These North American adjustments will be discussed in detail in the main paper on the global characteristics of the new model in Peltier *et al.* (2014). Secondly, in ICE-6G_C (VM5a) horizontal motion away from the centre of the Laurentide ice sheet is slower compared to the predictions of the ICE-5G (VM2) model to the south of the southern boundary of the Laurentide ice sheet over the continental United States, consistent with the space geodetic data (Peltier & Drummond 2008; Argus & Peltier 2010). In terms of lithosphere thickness, the most recent Toronto models differ considerably from their predecessors (e.g. Peltier 1984, 1986). In particular VM5a differs from VM2 in that the lower lithosphere consists of a 40-km thick layer having a high viscosity of 10^{22} Pa s which is overlain by a perfectly elastic layer of thickness 60 km and it is a consequence of this lithospheric stratification that the horizontal motion south of the area formerly covered by the ice sheet is well explained. Thirdly, ICE-6G_C (VM5a) has been modified from ICE-5G (VM2) so as to improve the fit to GPS uplift rates and geological observations in Antarctica, the documentation of which is the subject of this paper.

4.2 W12 and W12A

Whitehouse *et al.* (2012a) first estimated the W12 deglaciation history of Antarctica by fitting the 62 ice thickness change data based on exposure age dating that record the thickness of grounded ice at a sequence of times since Last Glacial Maximum. They furthermore maintained this model to be rational from a glacial dynamics perspective by using the Glimmer ice sheet model (Rutt *et al.* 2009) to test the ice thickness profiles in their reconstruction. Whitehouse *et al.* (2012b) next estimated an Earth model consistent with the

W12 deglaciation history by fitting 14 RSL histories along the Antarctica coast. They maintain, based on the RSL history data, that the viscosity of the upper mantle must be in the range of 0.8–2.0 × 10²¹ Pa s (95% confidence limits). We will show next that, on the contrary, an upper-mantle viscosity of 0.5 × 10²¹ Pa s, outside the 95% confidence limits of Whitehouse *et al.* (2012b), well fits the available data, including the RSL histories. Whitehouse *et al.* (2012b) then compared the postglacial rebound model based on the W12 deglaciation history and their Earth model to the 35 GPS uplift rates in Thomas *et al.* (2011).

Because the W12 model was found to overpredict the GPS inferred rates of uplift in the Antarctic Peninsula, and arguing that there have been large fluctuations in the amount of grounded ice on the Antarctic Peninsula in the late Holocene, Whitehouse *et al.* (2012b) generated a second model, denoted W12A. W12A differs from W12 in that this model has in the Antarctic Peninsula 150 m of ice gain from 1000 to 500 yr ago and a further 150 m of ice gain from 500 to 100 yr ago. This causes the predicted uplift in the peninsula to decrease by up to 5 mm yr⁻¹ in the transition from W12 to W12A.

In this study we will compare the Antarctic component of our ICE-6G_C (VM5a) model primarily to W12A simply because the W12A values of uplift have been made publicly available on a lat-lon grid throughout Antarctica. The W12 values of GPS inferred uplift rate are publicly available only for the 35 GPS sites in Thomas *et al.* (2011).

4.3 IJ_05 R2

We also compare against the IJ_05 R2 model of Ivins *et al.* (2013). In IJ05 R2 the contribution of Holocene Antarctic ice loss to global sea level rise is 7.5 m, similar to the 8 m value in W12 (Fig. 2). However, most ice loss in IJ05 R2 occurs later than in W12. Ivins *et al.* (2013) calculate vertical predictions based on two different Earth models. Their first Earth model has a lithosphere thickness of 115 km, an upper-mantle viscosity of 2 × 10²⁰ Pa s and a lower-mantle viscosity of 4 × 10²¹ Pa s. Their second Earth model has a lithospheric thickness of 65 km, an upper-mantle viscosity of 2 × 10²⁰ Pa s and a lower-mantle viscosity of 1.5 × 20²¹ Pa s. The two sets of predictions are similar, although the Earth model with the thinner elastic lithosphere yields more narrow areas of faster uplift.

4.4 A simple elastic model of current ice loss

To evaluate the solid Earth's elastic response to recent ice loss, we constructed an elastic model of current ice loss on the basis primarily of GRACE gravity data and secondarily on the ICE-6G_C (VM5a) postglacial rebound model (Figs S6 and S7). Our model has ice loss in two areas, in the Pine Island Bay region and in the Northern Antarctic Peninsula.

In the Pine Island Bay region, near the Amundsen Sea adjacent to West Antarctica, our model has a total of 143 Gt yr⁻¹ of ice loss. Using GRACE gravity data taken from 2003 to 2012, we estimate the mean rate of mass loss to be 124 Gt yr⁻¹. The rate of mass loss has increased over the time period, from 67 Gt yr⁻¹ from 2003 to 2007, to 190 Gt yr⁻¹ from 2008 to 2012. The correction for the solid Earth's uplift in viscous response to unloading of the ice-age ice sheets is calculated from the ICE-6G_C (VM5a) model to be 19 Gt yr⁻¹. The total ice loss of 143 Gt yr⁻¹ that we infer for the Pine Island, Thwaites and Smith Glaciers is 30 per cent larger than the

108 Gt yr⁻¹ inferred by King *et al.* (2012). This difference arises because we have employed two additional years of GRACE data, and because mass loss is inferred to have occurred at a faster rate in 2011 and 2012. The ICE-6G_C (VM5a) correction of 19 Gt yr⁻¹ is slightly larger than the W12A correction of 13 Gt yr⁻¹ employed by King *et al.* (2012).

In the Northern Antarctic Peninsula, our model has a total of 40 Gt yr⁻¹ of ice loss. Mass is observed with GRACE to decrease at a steady rate of 28 Gt yr⁻¹ from 2003 to 2012. The postglacial rebound correction calculated from ICE-6G_C (VM5a) is 12 Gt yr⁻¹. Ice loss in the Northern Peninsula is believed to be in response to the disappearance of the buttress provided by the Larsen B ice shelf, which broke up in 2002 February (Rott *et al.* 1998, 2002). Ice loss behind the former ice shelf is evident in fast uplift there at O'Higgins, Palmer, Rothera and several LARISSA sites.

Because we did not attempt to precisely specify the details of ice loss at Pine Island Bay and in the Northern Antarctic Peninsula, our model yields only rough predictions of uplift in these two areas of fast ice loss. In the Northern Antarctic Peninsula, our model predicts uplift to be a maximum of 7 mm yr⁻¹, or just half the fastest uplift rates observed (Table 1). At the three GPS sites near Pine Island Bay (Groh *et al.* 2012), our model predicts uplift at 12–23 mm yr⁻¹, at roughly the rates observed.

Our model is nevertheless instructive as a basis on which to evaluate the elastic contribution to uplift at GPS sites not near Pine Island Bay or the Northern Antarctic Peninsula. Elastic uplift elsewhere in West Antarctica exceeds 1 mm yr⁻¹ at four sites: 1.8 mm yr⁻¹ (Hown), 1.3 mm yr⁻¹ (Sdly), 1.3 mm yr⁻¹ (W06a) and 1.1 mm yr⁻¹ (Haag). Seven sites in West Antarctica have predicted uplift rates of 0.6–0.9 mm yr⁻¹. The remaining six sites have predicted uplift rates of 0.3–0.4 mm yr⁻¹.

Our elastic model of current ice loss predicts there to be more elastic uplift at the GPS sites near the Weddell Sea than the alternative model of Thomas *et al.* (2011, supporting text) based on the ICESat observations of Riva *et al.* (2009) (Fig. S8). This is primarily a consequence of the fact that their rate of ice loss near Pine Island Bay has increased since 2008, and our model includes a greater influence of this time of faster ice loss. We next use our model with faster elastic uplift to conservatively estimate the maximum effect of current ice loss at the GPS sites which are not in the near vicinity of these regions of current mass loss.

None of the nine GPS sites in the Northern Antarctic Peninsula were used to constrain postglacial rebound in ICE-6G_C (VM5a). Only the remaining 17 sites in West Antarctica and the 25 sites in East Antarctica are used to constrain ICE-6G_C (VM5a). The elastic model prediction for these 42 sites is sufficiently small that it makes little difference whether the observed uplift rate is corrected for the elastic model prediction. In the next section we will show explicitly that the weighted root mean square misfit of the ICE-6G_C (VM5a) model is insensitive to whether or not this elastic correction is made.

5 COMPARISONS BETWEEN MODELS AND DATA

5.1 Overall description of ICE-6G_C (VM5a) and W12A

In ICE-6G_C (VM5a) ice loss since Last Glacial Maximum is greatest in the interior of West Antarctica near 82°S 120°W (where the ice thickness has decreased by as much as 2500 m; Fig. S9). A second maximum in the loss of grounded ice occurs at the present-day

location of the Ronne–Filchner Ice Shelf (where the ice has thinned by up to 1500 m in the model). In ICE-6G_C (VM5a) the ice has also thinned by 100–500 m near the present-day coast of East Antarctica, where at LGM the grounded ice extended out to the shelf break (Denton & Hughes 1981). The interior of East Antarctica, however, is assumed not to have experienced either ice loss or gain since Last Glacial Maximum. Although it has been argued on the basis of the very small number of ice core records available from the plateau that thickening of ice has occurred in the interior of East Antarctica during the Holocene, the coverage of the entire area of the plateau is so sparse, no more than 2–3 widely spaced ice cores, that this conclusion should be viewed with caution.

Predictions of current uplift rates are similar in several respects between ICE-6G_C (VM5a) and W12A (Figs 6–8). Both models are characterized by two uplift extrema, one near the Ronne–Filchner Ice Shelf and the other near the Ross Ice Shelf, regions that were host at Last Glacial Maximum to significant grounded ice as a consequence of the fall in global sea level that accompanied the expansion of the great Northern Hemisphere ice sheets and which led to exposure of the shelves. These two locations of enhanced Antarctica ice mass at Last Glacial Maximum are essentially the same as those in the earlier reconstruction of the Antarctic ice sheet of Denton & Hughes (1981), which initially served as the basis for the locations of maximum ice loss in the Toronto ICE-NG sequence of deglaciation histories. Both models have slow uplift (1–3 mm yr^{-1}) near the East Antarctic coast and slow subsidence (0 to –2 mm yr^{-1}) in most of the East Antarctica interior. Both ICE-6G_C (VM5a) and W12A predict the coast adjacent to the Amundsen Sea to be rising quickly (at 5–7 mm yr^{-1}). In detail, the two models do differ significantly, however, as we will next proceed to describe.

5.2 Fit of ICE-6G_C (VM5a) to the GPS data

5.2.1 Summary

ICE-6G_C (VM5a) fits the observed GPS uplift rates well, mainly because we have revised the deglaciation history from ICE-5G to better fit the newly available data. Uplift due primarily to postglacial rebound is recorded at 42 sites not near Pine Island Bay or in the Northern Antarctic Peninsula. The wrms residual of the ICE-6G_C (VM5a) model to the 42 GPS uplift rates is 0.89 mm yr^{-1}. The weighted mean residual is –0.31 mm yr^{-1}, indicating that the model predicts slightly more uplift than observed. If we were to correct for our elastic model of current ice loss, the wrms residual would be 1.02 mm yr^{-1} and the weighted mean residual would be –0.48 mm yr^{-1}.

The W12A model of Whitehouse *et al.* (2012b) does not fit the vertical GPS data as well. The wrms residual of W12A to our 42 GPS uplift rates is 1.81 mm yr^{-1}. The weighted mean residual is –0.56, indicating that W12A also predicts more uplift than observed. If the elastic model were corrected for, the wrms would be 1.89 mm yr^{-1}, and the weighted mean residual would be –0.73 mm yr^{-1}. W12A poorly fits three GPS uplift rates. McMurdo is predicted to be rising at 3.7 mm yr^{-1}, significant faster than the 1.0 ± 1.2 mm yr^{-1} observed. W12A also overpredicts observed uplift at Crdi and Pece by 7–8 mm yr^{-1}. If these three data were omitted, then the wrms residual would fall to 1.31 mm yr^{-1}, still larger than the misfit of ICE-6G_C (VM5A).

The IJ05 R02 model of Ivins *et al.* (2013) also does not fit the vertical GPS data as well as ICE-6G_C (VM5A). Results for Ivins *et al.* (2013) two mantle viscosity profiles are similar. We next

quote residuals relative to their Earth model with a lithospheric thickness of 115 km. The wrms residual to our 42 GPS uplift data is 1.65 mm yr^{-1}. The weighted mean residual is 0.91 mm yr^{-1}, indicating that the model predicts less uplift than observed.

ICE-6G_C (VM5A) differs from ICE-5G (VM2) in that there is a total of 22 per cent less Antarctica ice loss since Last Glacial Maximum. The maximum predicted uplift southeast of Ross Ice Shelf decreases from 14 mm yr^{-1} to 11 mm yr^{-1} (compare fig. 2 of Argus *et al.* 2011 to Fig. 6 in this study). This reduction results from imposition of the constraints on ice thickness change derived from exposure age dating. The maximum predicted uplift south of the Ronne Ice Shelf increases slightly from 10 mm yr^{-1} to 11 mm yr^{-1}. Predicted uplift in the Southern Antarctic Peninsula decreases significantly from 10 mm yr^{-1} in our prior model to 5 mm yr^{-1} in our new model. This is due to Fossil Bluff's observed uplift rate of 2.9 ±2.3 mm yr^{-1} (Thomas *et al.* 2011).

5.2.2 Northern Antarctic Peninsula

Because the Northern Antarctic Peninsula is rising in elastic response to current ice loss, the nine sites from this region cannot be employed to usefully constrain our model of postglacial rebound. The GPS site Palmer exhibits a probable change in rate at the time of the break up of the Larsen B Ice Shelf in 2002 February (Thomas *et al.* 2011). In the 11 yr since that time Palmer has risen steadily at 7.7 ± 1.8 mm yr^{-1} (Fig. S2). In the 3.6 yr before the break up the site is estimated to have risen at 1.4 ± 5.4 mm yr^{-1} though this rate is clearly uncertain.

O'Higgins has risen at a mean rate of 4.9 ±1.4 mm yr^{-1} from 1993 to 2012. This uplift estimate is the mean based upon data from one VLBI site and three GPS sites. VLBI data record steady uplift at 4 ± 3 mm yr^{-1} from 1993 to 2004. The GPS site Ohig rose steadily at 4.8 ± 2.8 mm yr^{-1} from 1995 to 2001. (See also Domack *et al.* 2005.) This suggests that ice loss was occurring near O'Higgins before the break up of the Larsen B Ice Shelf. The GPS sites Ohi2 and Ohi3 rose at 5–7 mm yr^{-1} from 2003 to 2008, but uplift appears to have slowed to about 2 mm yr^{-1} from 2009 to 2012 (Fig. S2). GRACE does not record a diminishing rate of ice loss since 2009, though this would be difficult to resolve.

GPS site Frei, on the Shetland Islands, subsided at 2.9 ± 2.8 mm yr^{-1} from 1997 to 2004. This suggests that there was no ice loss in the Shetland Islands prior to the 2002 break up of the Larsen B Ice Shelf.

Rothera is observed to have risen steadily at 5.4 ± 2.7 mm yr^{-1} since 1999. This uplift estimate represents the weighted mean of GPS sites Rotb (12 yr of data) and Roth (3 yr of data; Fig. S2). Rotb is estimated to have risen at 4.3 ± 7.0 mm yr^{-1} in the 3 yr prior to the 2002 February break up of the Larsen B ice shelf, and therefore does not support the inference that the rate of ice loss from the Northern Peninsula increased subsequently.

5.2.3 Southern Antarctic Peninsula

We interpret uplift of GPS sites in the Southern Peninsula and along the south coast of the Weddell Sea to be due primarily to postglacial rebound rather than current ice loss. Fossil Bluff is rising at 2.9 ± 2.3 mm yr^{-1}, placing a tight constraint on postglacial rebound in the Southern Antarctic Peninsula (Figs 5–7). We have therefore greatly reduced ice loss since Last Glacial Maximum in ICE-6G_C relative to ICE-5G in the Southern Peninsula. Thomas *et al.* (2011) estimate Fossil Bluff's uplift rate to be 2.1 mm yr^{-1} (Table 2). We

estimate the uncertainty in this uplift rate to be ± 1.6 mm yr^{-1} for the time period of observation employed by Thomas *et al.* (2011). The uplift estimate of Thomas *et al.* (2011) is determined from the same three campaigns in 1996, 1998 and 2005 that we have employed, plus 1 yr of continuous data in 2010 that are unavailable to us. We deem the uncertainty in the Thomas *et al.* (2011) estimate to be less than the uncertainty in our estimate.

Near the base of the Antarctic Peninsula, we estimate Sugg to be rising at 5 mm yr^{-1} and Haag to be rising at 8 mm yr^{-1} (Figs 6–8 and Fig. S3). Our estimates of uplift are 4 mm yr^{-1} larger and more tightly constrained than those of Thomas *et al.* (2011).

ICE-6G_C (VM5a) predicts uplift in the Southern Antarctic Peninsula to be 3–7 mm yr^{-1} faster than in W12A (Figs 5–7). At Fossil Bluff and Sugg the observations lie between the predictions of the two models. W12 in turn differs from W12A in that it predicts uplift in the Southern Peninsula to be 5 mm yr^{-1} faster, owing to the 300 m of ice gain that is assumed to have occurred since 1 ka in W12A. Additional data from Fossil Bluff and Sugg would probably allow the ICE-6G_C (VM5a) and W12A models to be distinguished.

5.2.4 Weddell Sea

GPS data are providing important new constraints upon postglacial rebound models along the south coast of the Weddell Sea. Sites Hown, Wiln and W07 are all estimated to be rising at 5 mm yr^{-1}. In this area, our model differs from that of Whitehouse *et al.* (2012b) in two respects (Figs 5–7). First, ICE-6G_C (VM5a) predicts the uplift rate to be maximum at the centre of the Ronne Ice Shelf, whereas W12A predicts the uplift rate to be at its maximum 300 km south of the ice shelf (Fig. 6). Secondly, ICE-6G_C (VM5a) predicts the uplift rate to be nearly zero in the area between Wiln and Whtm, whereas W12A predicts the uplift rate to be 5–8 mm yr^{-1} in this region (Fig. 8). The observations cannot distinguish between the two models in this area, except that w06, based on just two campaigns separated by 3 yr, favours ICE-6G_C (VM5a).

Site Crdi is estimated to be rising at 2.8 ± 2.6 mm yr^{-1}, again favouring the 4 mm yr^{-1} in the ICE-6G_C (VM5a) model over the fast uplift rate of 7 mm yr^{-1} predicted by W12A. The estimated uplift rate at Pece also favours the slower rate predicted by our model over that of Whitehouse *et al.* (2012b), though Pece's estimated uplift rate is tenuous because the site is located near the edge of a cliff and exhibits large seasonal oscillations in the horizontal.

5.2.5 Ross Sea

McMurdo, on Ross Island along the west coast of the Ross Sea, is observed to be rising at 1.0 $\pm$ 1.2 mm yr^{-1}. The confidence limits are tight because this velocity is the mean of four GPS sites located within 3 km of each other (Crar, Sctb, Mcmd and Mcm4). The face-value estimate of uplift at each of the four sites is within 1 mm yr^{-1} of the mean. Site Crar has 10 yr of data with no discernable offset. Sites Mcm4 and Sctb have 5–6 yr of data without a break. The velocity of Mcm4 is not very tightly constrained because we estimate three offsets (not at times of logged antenna substitutions) over the 18-yr observation period.

McMurdo is 28 km from Mount Erebus, far enough from the volcano to not be significantly affected by its influence. Mount Erebus has been continuously active since 1972. Three GPS sites (Naus, E1g2 and Rayg) lie in the Erebus caldera and their motion

may reflect subsurface migration of magma. GPS site Hooz is 3 km west of the volcano.

W12A predicts McMurdo to be rising at 4 mm yr^{-1}, significantly faster than the rate observed with GPS. This misfit indicates that the model of Whitehouse *et al.* (2012b) has either too much ice loss along the west coast of the Ross Sea or that the viscosity of the upper mantle is too high. ICE-6G_C (VM5a) predicts current uplift to be 2 mm yr^{-1}, consistent with the observation. ICE-6G_C has maximum ice loss near the east coast of the Ross Sea, not near its centre as in W12A.

Twelve other GPS sites along the west coast of the Ross Sea have face-value uplift estimates of 2–3 mm yr^{-1}, but the confidence limits on these estimates (± 3–4 mm yr^{-1}) are loose because the sites have only 3–7 yr of available data. The uplift rate at site Ramg is observed to be 2.5 mm yr^{-1}, favouring the slow uplift of 4 mm yr^{-1} in ICE-6G_C (VM5a) over the fast uplift in W12A (at 7 mm yr^{-1}).

Site Patn, along the east coast of the Ross Sea, is rising at 5.5 $\pm$ 3.1 mm yr^{-1}, reflecting postglacial rebound (Fig. 6 and Fig. S3). This observation is consistent with the uplift rate of 4 mm yr^{-1} predicted by ICE-6G_C (VM5a) as well as that predicted by W12A (3 mm yr^{-1}). Patn's observed uplift is inconsistent with the interpretation of King *et al.* (2012) (and resulting modification of W12A) that uplift along the Siple coast is nearly zero.

5.2.6 East Antarctica

Uplift along the East Antarctic coast ranges from –0.5 to 1.5 mm yr^{-1}. Uplift is fastest at Vesleskarvet, Maitri and Casey (≈ 1.5 mm yr^{-1}). GRACE gravity data show that the coast of Queen Maud Land, East Antarctica, from 30°W to 60°E accumulated snow at 150 Gt yr^{-1} from 2009 January to 2013 February (Boening *et al.* 2012, this study), for a total of ≈ 600 Gt. Precipitation data also measure fast accumulation from 2009 to 2012, but measure accumulation to be zero from 1980 to 2008, showing the recent snow accumulation to be anomalous and to represent interannual variation (Boening *et al.* 2012). The loading from 2009 to 2012 must cause the coast to subside. The subsidence inferred from GRACE near Syowa and Maitri using equation 6 of Kusche & Schrama (2005) is about –2 mm yr^{-1}, for a total subsidence of 8 mm from 2009 to 2012. An elastic model of ice accumulation that we have constructed on the basis of ice gain of 150 Gt yr^{-1} estimated from GRACE data from 2009 to 2012 yields faster, more local subsidence of up to –4.5 mm yr^{-1} near Syowa, Maitri and Vesleskarvet. The predicted total subsidence of –8 to –15 mm cannot, however, be readily resolved in the time-series for Syowa. The series at Vesleskarvet is inconclusive, showing a possible slow down in uplift beginning around 2008, but also a speed up around 2002. In summary, the rates of uplift observed along the coast of East Antarctica require postglacial rebound in this region to be small.

5.3 The fit of ICE-6G_C (VM5a) to the ice thickness change data

5.3.1 Summary

We next compare predictions of the ICE-6G_C (VM5a) model to the 62 estimates of ice thickness change at 20, 15, 10 and 5 ka that were carefully analysed and compiled by Whitehouse *et al.* (2012a) (Fig. 1). In the upper plates of Figs 12(a)–(c) the exposure age constraints on ice thickness change are plotted against the predictions of ICE-6G_C (VM5a; blue curves) and W12 (orange X's); in the
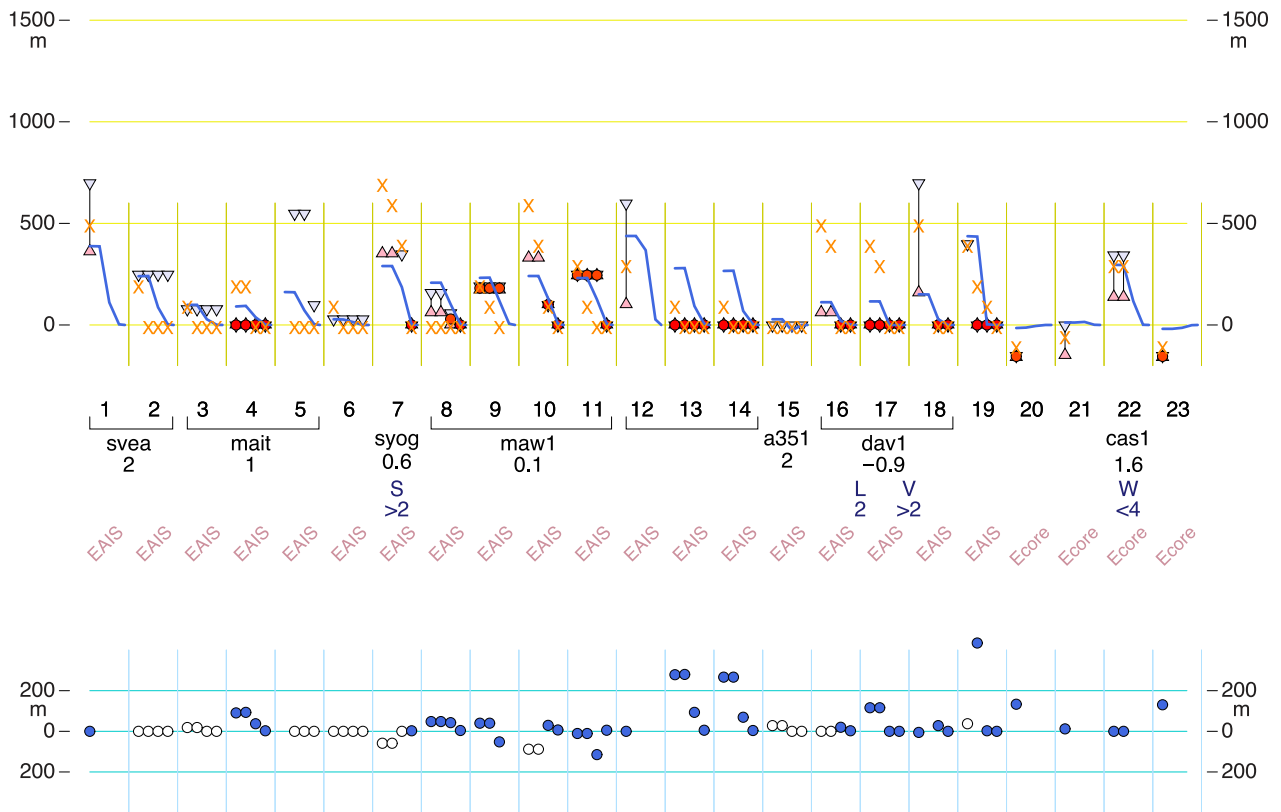
Figure 12. Estimates of ice thickness change at 20, 15, 10 and 15 ka are compared with model predictions. Fig. 11 shows the locations of the data, 1–62, which are from Whitehouse *et al.* (2012a). At top red circles show estimates with upper and lower bounds. Upright triangles show lower bounds; inverted triangles show upper bounds. For some data, in particular those requiring zero ice height change, the error bars are so tight that both triangles are nearly entirely beneath the red circle. Blue curves show ice height changed predicted by ICE-6G (VM5a). Orange X's show ice change predicted by W12 (Whitehouse *et al.* 2012a). Horizontal line segments beneath the data numbers group nearby sites; the name and uplift rate of nearby GPS sites are given, and rates of relative sea level fall at nearby sites are also given. At bottom are residuals relative to ICE-6G (VM5a). Blue circles are data with both upper and lower bounds; open circles show data with either an upper bound or a lower bound.

bottom charts the residuals of the geological data relative to ICE-6G_C (VM5a) are plotted. (The blue circles are sites with upper and lower geological bounds on ice thickness change, whereas the open circles are sites having either an upper bound or a lower bound.) Sites 1–23 are in East Antarctica, sites 24–42 are near the Ross Sea and sites 43–62 are in West Antarctica. At each site ice thickness change is plotted at four times (if available): 20 ka, 15 ka, 10 ka and 5 ka. In ICE-6G_C (VM5a) ice thickness decreases quickly from 12 ka to 5 ka (so that the blue curves have steep slopes.) Groups of nearby sites are indicated by the horizontal line segments beneath the site names. Also shown in Fig. 12 are nearby estimates of uplift rate from GPS and estimates of RSL fall from geological data.

ICE-6G_C (VM5a) fits 93 per cent of the ice thickness change data within 200 m, comparable to the 85 per cent fit within 200 m achieved by W12. There are no systematic differences between ICE-6G_C (VM5a) and the data. The largest misfits are located in two regions. Along the coast of east Lambert Bay (sites 13,14), ICE-6G_C (VM5a) has 270 m of ice loss since Last Glacial Maximum, misfitting the observations of zero at sites 13 and 14. ICE-6G_C (VM5a) has no ice is loss in Antarctica after 4 ka, and thus misfits the estimates of ice loss in Marie Byrd Land since 5 ka of 400 m at site 45 and 290 m at site 46.

At some sites ICE-6G_C (VM5a) may misfit the ice thickness change and RSL data simply because the topographic detail is not well represented by the 55–110 km spatial resolution in ICE-6G. The

ice thickness changes in the model must be interpreted as representing the average over the surrounding region and may be expected to differ from the actual changes in areas of rugged topography. It must also be recognized that the interpretation of the meaning of the exposure age dates is also subject to significant uncertainty and so it is not possible to ascribe precise quantitative meaning to them.

5.3.2 The usefulness of ice core estimates on ice thickness change in the interior of East Antarctica

The two postglacial rebound models differ markedly in Coats Land near 80°S 15°E. W12A predicts subsidence there at rates up to −6 mm yr^{-1}, in viscous response to the ≈200 m of ice gain assumed to have occurred in the model since 5 ka. This fast subsidence is not strongly constrained on the basis of ice physics. In W12 the ice gain that is assumed to have occurred in Coats Land since Last Glacial Maximum is acknowledged to be very uncertain (fig. 6 of Whitehouse *et al.* 2012a).

At the three ice core sites in the interior of East Antarctica, ICE-6G_C (VM5a) has essentially zero ice thickness change, disagreeing with the 150 m of ice gain inferred at Dome Fuji (site 20) and EPICA Dome C (site 23). No uncertainty is assigned to these hypothetical increases in ice thickness at Dome Fuji and Dome C in the study of Parrenin *et al.* (2007). At Dome Vostok (site 21), ICE-6G_C (VM5a) has zero ice thickness change, fitting the inferred
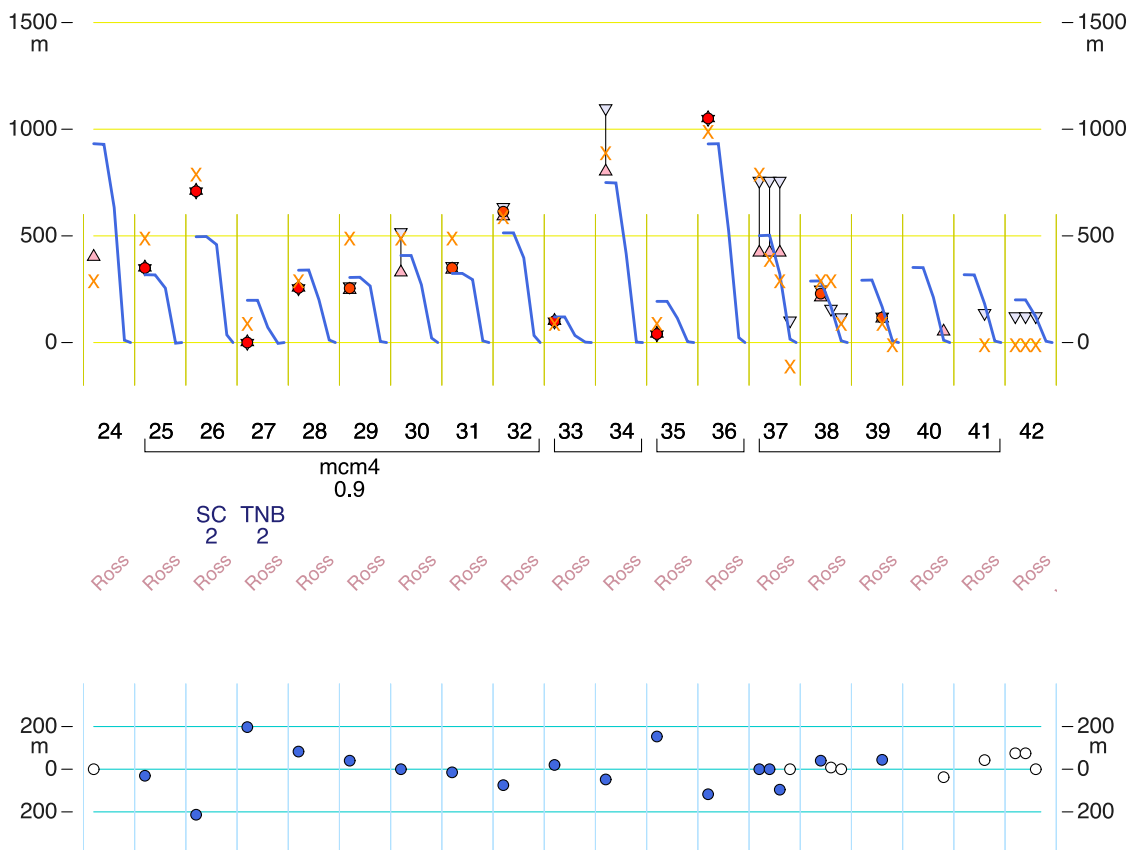
Figure 12. (*Continued.*)

ice thickness change within the error bars. In fact, there is no direct connection between isotopic data from ice cores and ice thickness change because such data constrain only accumulation and the inference of accumulation is necessarily indirect. Former ice thickness at Beardmore Glacier, an outlet through the Transantarctic Mountains, has been proposed to constrain ice thickness in the East Antarctic interior at the Last Glacial Maximum (Denton & Hughes 1981). Beardmore Glacier was close to its current elevation in its upper reaches (ice thickness change datum 35, Fig. 1) and considerably thicker in its middle and lower reaches (datum 36) during the last two global glaciations. This implies that elevations of the polar plateau near Titan Dome has changed little since Last Glacial Maximum (Denton & Hughes 1981). Our inability to accurately infer either a gain or a loss of ice mass from the plateau as a whole since LGM will oblige us to perform a detailed sensitivity analysis of the impact of this influence upon our inference of the contribution of Antarctica to modern global sea level rise based upon GIA corrected GRACE gravity observations.

5.4 The fit of ICE-6G_C (VM5a) to the RSL data

5.4.1 Summary

Geological estimates of the average rate of RSL change at 12 places along the coast of Antarctica range from 1 to 4 mm yr^{-1} (Figs 11 and 13). Global sea level has not risen appreciably since 4 ka (Peltier 2002; Peltier *et al.* 2002). This conclusion is based primarily on RSL observations from islands in the equatorial Pacific that record a mid-Holocene high stand of the sea, a feature that is accurately

predicted when Antarctic deglaciation is assumed to have ceased at 4 ka according to the previous ICE-5G (VM2) model. This suggests that the observed RSL fall along the Antarctica coast is due mainly to the rise of the land associated with the postglacial rebound process. The sparseness of the data, however, limits their usefulness. The 12 RSL histories that we examine in this study (Fig. 13) are nearly identical to the 14 used by Whitehouse *et al.* (2012b, fig. 3). (We omit Rauer, a RSL history with just three data in the time period between 14 ka and 9 ka. We also include in our South Shetland Islands history nearby RSL data from Byers Peninsula and Fildes Peninsula.)

Whitehouse *et al.* (2012b) maintain that the RSL histories require the upper-mantle viscosity to lie in the range 0.8–2.0 × 10^{21} Pa s. We do not find this conclusion to be consistent with the results of our own analysis. ICE-6G_C (VM5a) fits all 12 RSL histories rather well. For each RSL history, the lower value of the viscosity of the upper mantle in VM5a is being compensated by larger ice loss since Last Glacial Maximum in ICE-6G. W12A nevertheless poorly fits the RSL history at Marguerite Bay, where it predicts RSL to have fallen at an average rate of 6 mm yr^{-1}, three times faster than the observed rate of 2 mm yr^{-1}. On the other hand, ICE-6G_C (VM5a) well fits the RSL curve at Marguerite Bay.

5.4.2 East Antarctica

Four RSL histories along the East Antarctica coast suggest that RSL has fallen at an average rate of at least 2 mm yr^{-1} over the past several thousand years.

Along the Soya coast, RSL has fallen by at least 6 m since 3 ka, for an average rate of 2 mm yr^{-1}. Some sea level data in our
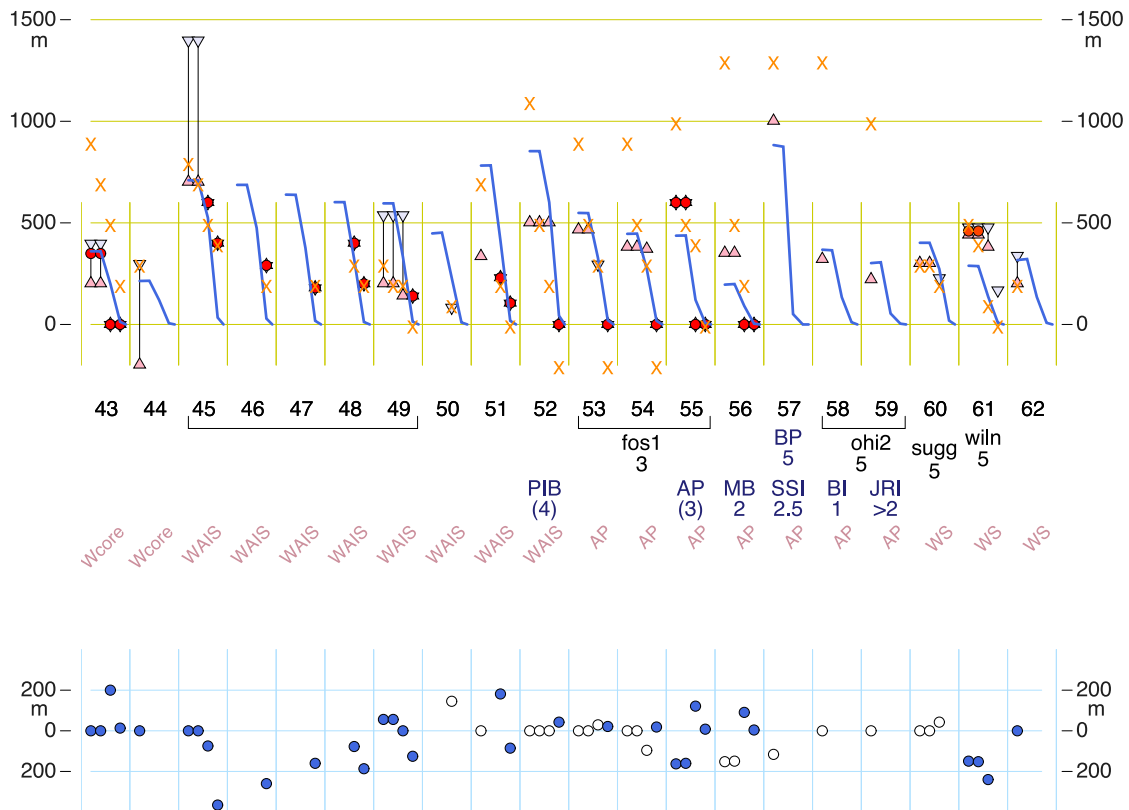
Figure 12. (*Continued.*)

compilation but not in that of Whitehouse *et al.* (2012b) suggest that sea level may have fallen further over the same time period. ICE-6G_C (VM5a) and W12 predict that sea level has fallen by 6 m since 3 ka, misfitting some of the data.

At Vestfold Hills, RSL has fallen about 4 m since 4 ka, for an average rate of $\approx 1\,\mathrm{mm\,yr^{-1}}$. ICE-6G_C (VM5a) and W12 well fit this RSL history. At Larsemann Hills, RSL has fallen by $\approx 6\,\mathrm{m}$ since 3 ka, for an average rate of $2\,\mathrm{mm\,yr^{-1}}$. ICE-6G_C (VM5a) and W12 both fit this RSL history as well. At Windmill Islands, RSL has fallen ≈ 25 m, and again ICE-6G_C (VM5a) and W12 both adequately fit this RSL history.

5.4.3 Ross Sea

At Terra Nova Bay, RSL has fallen about 6 m over the past 3 ka, for an average rate of about $2\,\mathrm{mm\,yr^{-1}}$. The RSL data require a slight decrease in the rate of sea level fall with time. Curvature is clearly required by the available sea level data and the rate must have been $\approx 3\,\mathrm{mm\,yr^{-1}}$ from 6 ka to 3 ka. ICE-6G_C (VM5a) predicts this RSL history very well, whereas W12 predicts RSL to have fallen slightly more quickly than observed.

Along the Scott Coast, RSL has also fallen by ≈ 6 m over the past 3 ka, for an average rate of about $2\,\mathrm{mm\,yr^{-1}}$. ICE-6G_C (VM5a) and W12 fit the data well, except that the two models predict sea level to have fallen slightly more (18 m) than observed (12 m) since 6 ka.

5.4.4 Antarctic Peninsula

There are two RSL curves available from the Southern Antarctic Peninsula. RSL along the Marguerite Bay coast has fallen by 8 m

since 4 ka, for a rate of $2\,\mathrm{mm\,yr^{-1}}$. ICE-6G_C (VM5a) predicts sea level to have fallen by 8 m since 4 ka, fitting the datum. On the other hand, W12 predicts sea level to have fallen by 24 m since 4 ka, a factor of 3 greater than observed. Because this datum is fit so badly, Whitehouse *et al.* (2012b) omit it from their inversion for mantle viscosity.

At Ablation Point, a single beach marker suggests that RSL has fallen by 15 m since 5 ka, for an average rate of $3\,\mathrm{mm\,yr^{-1}}$. ICE-6G_C (VM5a) predicts RSL to have fallen by 25 m since 5 ka, 10 m more than observed. The W12 model, however, predicts sea level to have fallen by 40 m since 5 ka, 25 m more than observed.

At three locations near the tip of the Antarctic Peninsula, estimates of the average rate of RSL fall range from 1 to $2.5\,\mathrm{mm\,yr^{-1}}$. In the South Shetland Islands, RSL has fallen by 15 km since 6 ka, for a rate of $2.5\,\mathrm{mm\,yr^{-1}}$. ICE-6G_C (VM5a) predicts sea level to have fallen slightly more slowly than observed, whereas W12 fits the datum. At Beak Island, RSL has fallen just 3 m since 3 ka, for a rate of $1\,\mathrm{mm\,yr^{-1}}$, ICE-6G_C (VM5a) predicts sea level to have fallen slightly more quickly than observed, whereas W12 fits the datum. At James Ross Island, RSL has fallen by at least 15 m since 6 ka, for a minimum rate of $2.5\,\mathrm{mm\,yr^{-1}}$. ICE-6G_C (VM5a) predicts that sea level has fallen 12 m since 6 ka, slightly less than observed.

6 DISCUSSION

6.1 Uncertainty in the postglacial rebound model

While we would like to quantify the uncertainty in the postglacial rebound model, this is extremely difficult to do. The full covariance
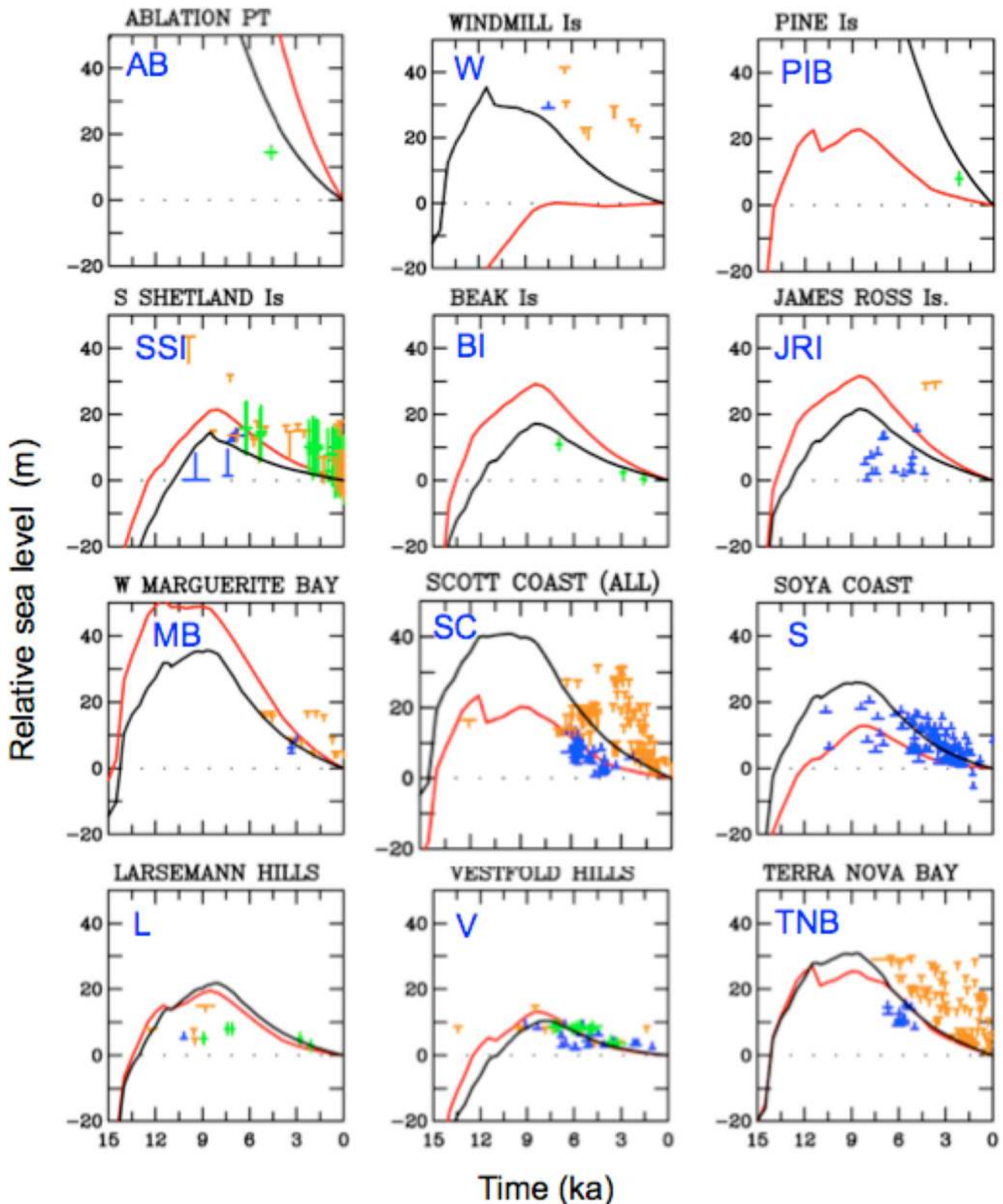
Figure 13. Relative sea level (RSL) histories at 12 sites. Small orange bars show upper limits on RSL. Blue bars show lower limits. Green bars have upper and lower limits. The black curve is the prediction of ICE-6G C (VM5a). The red curve is the prediction of ICE-5G v1.3 (VM2). Fig. 1 shows the site locations.

between the deglaciation history and mantle viscosity profile would have to be explored. That is, it is insufficient to vary just one of the two parameters within that parameter's uncertainty; both parameters must be varied.

Moreover, we maintain that published estimates of uncertainties are unrealistically small given the range of parameters in the three Antarctic postglacial rebound models. Estimates of the upper-mantle viscosity (the pertinent parameter for the Antarctica ice

sheet) disagree markedly. Values of upper-mantle viscosity, in units of 10^{20} Pa s, are: 8–20 (W12A, Whitehouse *et al.* 2012b), 5 (VM5a, this study) and 1.5–3 (IJ05 R2, Ivins *et al.* 2013). The bounds quoted for Whitehouse *et al.* (2012b) and for Ivins *et al.* (2013) are 95% confidence limits. Hence, the W12A and IJ05 R2 studies infer uncertainty in the postglacial rebound model from these significantly different values of upper-mantle viscosity. The upper mantle viscosity in either W12 or IJ05 R2 must be incorrect.

The three deglaciation histories also differ significantly. IJ05 R2 differs strikingly from W12 in that ice loss in IJ105 R2 comes much later than in W12. IJ05 R2 and W12 differ by 5 m in the time period from 11.5 to 7 ka. And of course ICE-6G_C has 70 per cent more total ice loss than either W12 or IJ05 R2.

6.2 Postulated West Antarctica phenomena

A range of phenomena are postulated to have occurred in West Antarctica over the past 1000 yr. In the model of Ivins & James (2005), loss of grounded ice from West Antarctica over the past 150 yr is assumed to have raised global sea level 0.080 m, at a rate of 0.5 mm yr^{-1}. Earth's surface would rise at up to 20 mm yr^{-1} in viscous response to such rapid ice loss (Simon *et al.* 2010, fig. 3a), a prediction that is ruled out by the GPS uplift observations.

On the other hand Whitehouse *et al.* (2012b) postulate that ice in the Antarctic Peninsula thickened significantly over the past 1000 yr. Model W12A differs from model W12 in that in W12A ice in the Antarctic Peninsula thickened by 300 m from 1000 to 100 yr ago. Such thickening would cause the peninsula to subside by up to 5 mm yr^{-1}. On the basis of ice core observations Nield *et al.* (2012) postulate that an increase in snow accumulation thickened the ice sheet near the west coast of the Antarctic Peninsula by up to 45 m since 1850, consistent with W12A.

Ivins *et al.* (2013) maintain that the Antarctic Peninsula has risen over the past 150 yr in viscous response to unloading of ice after the Little Ice Age, which occurred from 1550 to 1850. They postulate that the viscous response of the Antarctic Peninsula to Little Ice Age deglaciation is described by a characteristic time of just a few hundred years because the viscosity of the upper mantle is low (5×10^{19}) due to the proximity of seafloor spreading centres. Ivins *et al.* (2013) thus postulate that current uplift in viscous response to Little Ice Age deglaciation is significant.

GPS uplift rates that are faster than expected are motivation for ice thickening and Little Ice Age viscous response in the Antarctic Peninsula. We find, however, the GPS estimates of uplift to be consistent with that expected from current ice loss and postglacial rebound in ICE-6G VM5a. We find GPS residuals relative to the sum to be close to zero: –1.1 mm yr^{-1} (O'Higgins), 2.1 (Palmer), 2.1 (Rothera) and –1.8 mm yr^{-1} (Fossil Bluff).

6.3 Consistency with ice physics

As we state in the Methods section, we have not explicitly sought to make ICE-6G_C fully consistent with expectations based upon a particular representation of ice mechanical processes. In our opinion this would inappropriately restrict the space of plausible deglaciation histories as the inferred history would then depend upon both the details of the representation of ice mechanical processes selected (shallow ice, shelfy stream, full Stokes, etc.), and the climate (including sea level) forcing to which the model is subject. In our model the total topography, equal to bedrock elevation plus ice sheet thickness, is nevertheless reasonably smooth at Last Glacial Maxi-

mum (Fig. S10). Work is nevertheless ongoing to construct a range of ice sheet models that could be consistent with the GIA inferred history upon which we have focused in the current paper.

7 CONCLUSIONS

We are led to the following conclusions on the basis of the analyses discussed in the previous sections of this paper:

(1) ICE-6G_C (VM5a) well fits the available GPS uplift rates, estimates of ice thickness changes from exposure dating, and RSL histories. The wrms misfit of the 42 GPS uplift rates that are insignificantly affected by current ice loss is 0.89 mm yr^{-1}, which is half the 1.81 mm yr^{-1} misfit of model W12A.

(2) Uplift in elastic response to current ice loss is quite fast but highly localized near Pine Island Bay and adjacent to the Larsen Ice Shelf. Whereas the Northern Antarctic Peninsula and the Amundsen Sea coast are strongly influenced by current ice loss, most of Antarctica, including the Southern Antarctic Peninsula and Weddell Sea coast, is not. Thus, GPS uplift rates in most areas of Antarctica strongly constrain postglacial rebound.

(3) The southern margins of the Ronne and Ross Ice Shelves are observed with GPS to be moving horizontally away from the shelf centres at 0.5–1.0 mm yr^{-1}. This slow horizontal motion is the solid Earth's viscous response to early Holocene unloading of grounded ice from the current location of the two ice shelves.

(4) Uplift due to postglacial rebound is observed to be fastest (5–8 mm yr^{-1}) near the Ellsworth Mountains and along the south coast of the Weddell Sea. The west coast of the Ross Sea is rising at 1–3 mm yr^{-1}, whereas the northeast coast of the Ross Sea is rising at 5.5 mm yr^{-1}.

(5) The overall uplift rate of Antarctica is similar in models ICE-6G_C (VM5a) and W12A. There are, however, large local differences of +8 mm yr^{-1} in Coats Land, +8 mm yr^{-1} in the Southern Antarctic Peninsula, +9 mm yr^{-1} in the Antarctic interior near 82°S 120°W and –8 mm yr^{-1} in the West Antarctica interior near 82°S 90°W (Figs 9 and 11). Positive values indicate the uplift rate is greater in ICE-6G_C (VM5a) than in W12A.

(6) Whitehouse *et al.* (2012b) maintain that the available Antarctica RSL histories constrain the viscosity of the upper mantle to be 0.8 to 2.0 × 10^{21} Pa s (95% confidence limits). We find, on the contrary, that an upper-mantle viscosity of 0.5 × 10^{21} Pa s, can well fit all available data, including RSL histories, when coupled with a deglaciation history in which ice loss is characterized by a contribution to global sea level rise of 13.6 m occurring from 14 to 5 ka.

(7) In ICE-6G_C Antarctic ice loss raised global sea level by 13.6 m since Last Glacial Maximum, 70 per cent more than the 8 m in W12A. Moreover, in ICE-6G_C Antarctica ice loss at the time of Meltwater Pulse 1B (11.5 ka) raised global sea level by ≈5 m, contributing significantly to the strong increase in RSL that occurred at this time that is recorded by the Barbados coral record of Peltier & Fairbanks (2006). The timing of the onset of most rapid deglaciation of Antarctic in ICE-6G_C is consistent with the constraints provided by sedimentary core data from the continental shelf surrounding the continent. The W12 and W12A models are not consistent with these data.

(8) In ICE-6G_C the viscous response of the solid Earth to early Holocene ice loss is increasing gravity by a mass equivalent of 107 Gt yr^{-1}. In most places in Antarctica the gravity increase in ICE-6G_C is similar to that in W12A. In the interior of East Antarctica, however, gravity increase in ICE-6G_C is 2 Gt yr^{-1}, differing significantly from the gravity decrease of 21 Gt yr^{-1} in W12A.

(9) Whitehouse *et al.* (2012a,b) maintain the contribution of the post-LGM deglaciation of Antarctica to global sea level rise is just 8 m, less than half that (17.5 m) in ICE-5G (VM2). This finding is being used to infer that more ice must have been lost from North America and Northern Europe since Last Glacial Maximum (*cf.* Austermann *et al.* 2013). In this study we infer Antarctica ice loss to have contributed 13.6 m to global sea level rise, just 20 per cent less than the 17.5 m in ICE-5G (VM2). Our global ICE-6G (VM5a) model continues to fit the Barbados data set very accurately given that adjustments to Northern Hemisphere ice cover that have also been required to fit the new set of space geodetic observations. We maintain total Antarctic ice loss in the model of Whitehouse *et al.* (2012b) to be too small because the mantle viscosity in their model is too high. The model of Whitehouse *et al.* (2012b) furthermore does not satisfy constraints on timing of the onset of marine sedimentation on the continental shelf indicating increased Antarctic ice loss from 12 to 7 ka. This underscores the relationship between the amount of ice loss, its timing, and the relaxation time that governs the viscous response of the solid Earth to deglaciation.

ACKNOWLEDGEMENTS

REFERENCES

A, G., Wahr, J. & Zhong, S., 2013. Computations of the viscoelastic response of a 3-D compressible Earth to surface loading: an application to Glacial Isostatic Adjustment in Antarctica and Canada, *Geophys. J. Int.,* **192,** 557–572.

Altamimi, Z., Collilieux, X. & Métivier, L., 2011. ITRF2008: an improved solution of the international terrestrial reference frame, *J. Geodyn.,* **85,** 457–473.

Altamimi, Z., Métivier, L. & Collilieux, X., 2012. ITRF2008 plate motion model, *J. geophys. Res.,* **117,** B07402, doi:10.1029/2011JB008930.

Argus, D.F., 2007. Defining the translational velocity of the reference frame of Earth, *Geophys. J. Int* **169,** 830–838.

Argus, D.F., 2012. Uncertainty in the velocity between the mass center and surface of Earth, *J. geophys. Res.,* **117,** B10405, doi:10.1029/2012JB009196.

Argus, D.F. & Gross, R.S., 2004. An estimate of motion between the spin axis and the hotspots over the past century, *Geophys. Res. Lett.,* **31,** L06614, doi:10.1029/2004GL019657.

Argus, D.F. & Peltier, W.R., 2010. Constraining models of postglacial rebound using space geodesy: a detailed assessment of model ICE-5G (VM2) and its relatives, *Geophys. J. Int.,* **181,** 697–723.

Argus, D.F., Blewitt, G., Peltier, W.R. & Kreemer, C., 2011. Rise of the Ellsworth Mountains and parts of the East Antarctic coast observed with GPS, *Geophys. Res. Lett.,* **38,** L16303, doi:10.1029/2011GL048025.

Argus, D.F., Gordon, R.G., Heflin, M.B., Ma, C., Eanes, R.J., Willis, P., Peltier, W.R. & Owen, S.E., 2010. The angular velocities of the plates and the velocity of Earth's center from space geodesy, *Geophys. J. Int.,* **180,** 913–960.

Argus, D.F., Peltier, W.R. & Watkins, M.M., 1999. Glacial isostatic adjustment observed using very long baseline interferometry and satellite laser ranging, *J. geophys. Res.,* **104,** 29 077–29 093.

Austermann, J., Mitrovica, J.X., Latychev, K. & Milne, G.A., 2013. Barbados-based estimate of ice volume at Last Glacial Maximum affected by subducted plate, *Nat. Geosci.,* **6,** 553–557.

Bard, E., Hamelin, B. & Delanghe-Sabatier, D., 2010. Deglacial Meltwater Pulse 1B and Younger Dryas Sea Levels Revisited with Boreholes at Tahiti, *Science,* **327,** 1235–1237.

Bentley, M.J., Fogwill, C.J., Le Brocq, A.M., Hubbard, A.L., Sugden, D.E., Dunai, T.J. & Freeman, S.P.H.T., 2010. Deglacial history of the West Antarctic Ice Sheet in the Weddell Sea embayment: Constraints on past ice volume change, *Geology,* **38,** 411–414.

Bevis, M. *et al.*, 2009. Geodetic measurements of vertical crustal velocity in West Antarctica and the implications for ice mass balance, *Geochem. Geophys. Geosyst.,* **10,** 311–321.

Bevis, M., Brown, A. & Kendrick, E., 2013. Devising stable geometrical reference frames for use in geodetic studies of vertical crustal motion, *J. Geod.,* **87,** 311–321.

Boehm, J., Mendes Cerveira, P.J., Schuh, H. & Tregoning, P., 2007. The impact of mapping functions for the neutral atmosphere based on numerical weather models in GPS data analysis, in *Dynamic Planet—Monitoring and Understanding a Dynamic Planet With Geodetic and Oceanographic Tools, Int. Assoc. Geod. Symp.,* Vol. **130,** pp. 837–843, eds Tregoning, P. & Rizos, C., Springer.

Boehm, J., Niell, A., Tregoning, P. & Schuh, H., 2006a. Global Mapping Function (GMF): a new empirical mapping function based on numerical weather model data, *Geophys. Res. Lett.,* **33,** L07304, doi:10.1029/2005GL025546.

Boehm, J., Werl, B. & Schuh, H., 2006b. Troposphere mapping functions for GPS and very long baseline interferometry from European Centre for Medium-Range Weather Forecasts operational analysis data, *J. geophys. Res.,* **111,** B02406, doi:10.1029/2005JB003629.

Boening, C., Lebsock, M., Landerer, F. & Stephens, G., 2012. Snowfall-driven mass change on the East Antarctic ice sheet, *Geophys. Res. Lett.,* **39,** L21501, doi:10.1029/2012GL053316.

Capra, A., Mancini, F. & Negusini, M., 2007. GPS as a geodetic tool for geodynamics in northern Victoria Land, Antarctica, *Antarctic Science,* **19,** 107–114.

Chambers, D.P., Wahr, J., Tamisiea, M.E. & Nerem, R.S., 2010. Ocean mass from GRACE and glacial isostatic adjustment, *J. geophys. Res.,* **115,** B11415, doi:10.1029/2010JB007530.

Chambers, D.P., Wahr, J., Tamisiea, M.E. & Nerem, R.S., 2012. Reply to comment by W. R. Peltier *et al.* on "Ocean mass from GRACE and glacial isostatic adjustment", *J. geophys. Res.,* **117,** B11404, doi:10.1029/2012JB009441.

Chen, J.L., Wilson, C.R., Blankenship, D. & Tapley, B.D., 2009. Accelerated Antarctic ice loss from satellite gravity measurements, *Nat. Geosci.,* **2,** 859–862.

Craymer, M., Henton, J.A., Piraszewski, M. & Lapelle, E., 2011. An updated GPS velocity field for Canada, Abstract G21A-0793, *American Geophysical Union,* Dec. 5–9, San Francisco.

Denton, G.H. & Hughes, T.J., eds., 1981. *The Last Great Ice Sheets,* 484 pp. plus maps, John Wiley.

Desai, S.D. *et al.*, 2009. The JPL IGS analysis center: results from the reanalysis of the global GPS network, Abstract G18B-0630 presented at 2009 Fall Meeting, *American Geophysical Union,* Dec. 6–11, San Francisco, CA.

Desai, S.D., Bertiger, W., Haines, B., Harvey, N., Sella, C., Sibthorpe, A. & Weiss, J.P., 2011. Results from the reanalysis of global GPS data in the IGS08 reference frame, Abstract G53B-0904 presented at 2011 Fall Meeting, *American Geophysical Union,* Dec. 5–9, San Francisco, CA.

Deblonde, G. & Peltier, W.R., 1991, Simulations of continental ice sheet growth over the last glacial-interglacial cycle: experiments with a one-level seasonal energy balance model including realistic geography, *J. geophys. Res.,* **96**(D5), 9189–9215.

Deblonde, G. & Peltier, W.R., 1992. Simulations of continental ice sheet growth over the last glacial-interglacial cycle: experiments with a one-level seasonal energy balance model including seasonal ice albedo feedback, *Glob. planet. Change,* **98**, 37–55.

Deblonde, G. & Peltier, W.R., 1993. Late Pleistocene ice-age scenarios based on observational evidence, *J. Clim.,* **6**, 709–727.

Domack, E. *et al.*, 2005. Stability of the Larsen B Ice Shelf on the Antarctic Peninsula during the Holocene epoch, *Nature,* **436**, 681–685.

Dyke, A.S. & Prest, V.K., 1987. Late Wisconsinan and Holocene history of the Laurentide ice sheet, *Géographie physique et Quaternaire,* **41**, 237–263.

Gazeaux, J. *et al.*, 2013. Detecting offsets in GPS time series: first results from the detection of offsets in GPS experiment, *J. geophys. Res. Solid Earth,* **118**, 2397–2407.

Groh, A., Ewert, H., Scheinert, M., Fritsche, M., Rülke, A., Richter, A., Rosenau, R. & Dietrich, R., 2012. An investigation of Glacial Isostatic Adjustment over the Amundsen Sea sector, West Antarctica, *Glob. Planet. Change,* **98–99**, 45–53.

Gross, R.S. & Vondrak, J., 1999. Astrometric and space-geodetic observations of polar wander, *Geophys. Res. Lett.,* **26**, 2085–2088.

Horwath, M. & Dietrich, R., 2009. Signal and error in mass change inferences from GRACE: the case of Antarctica, *Geophys. J. Int.,* **177**, 849–864.

Ivins, E.R. & James, T.S., 2005. Antarctic glacial isostatic adjustment: a new assessment, *Antarc. Sci.,* **17**, 541–553.

Ivins, E.R., James, T.S., Wahr, J., Schrama, E.J.O., Landerer, F.W. & Simon, K.M., 2013. Antarctic contribution to sea level rise observed by GRACE with improved GIA correction, *J. geophys. Res.,* **118**, 3126–3141.

King, M.A., Bingham, R.J., Moore, P., Whitehouse, P.L., Bentley, M.J. & Milne, G.A., 2012. Lower satellite-gravimetry estimates of Antarctic sea-level contribution, *Nature,* **491**, 586–589.

Kusche, J. & Schrama, E.J.O., 2005. Surface mass redistribution inversion from global GPS deformation and Gravity Recovery and Climate Experiment (GRACE) gravity data, *J. geophys. Res.,* **110**, B09409, doi:10.1029/2004JB003556.

Larson, K.M., 2013. A methodology to eliminate snow- and ice-contaminated solutions from GPS coordinate time series, *J. geophys. Res.,* **118**, 4503–4510.

Larson, K.M. & Nievinski, F.G., 2012. GPS snow sensing: results from the EarthScope Plate Boundary Observatory, *GPS Solutions* **17**, 41–52.

Leventer, A. *et al.*, 2006. Marine sediment record from the East Antarctic margin reveals dynamics of ice sheet recession, *GSA Today,* **16**, 4–10.

Lidberg, M., Johansson, J.M., Scherneck, H.-G. & Milne, G.A., 2010. Recent results based on continuous GPS observations of the GIA process in Fennoscandia from BIFROST, *J. Geodyn.,* **50**, 8–18.

Mackintosh, A. *et al.*, 2011. Retreat of the East Antarctic ice sheet during the last glacial termination, *Nat. Geosci.,* **4**, 195–202.

Mackintosh, A.N. *et al.*, 2013. Retreat history of the East Antarctic Ice Sheet since the Last Glacial Maximum, *Quat. Sci. Rev.,* **33**, 1–21.

McConnell, R.K., 1968. Viscosity of the mantle from relaxation time spectra of isostatic adjustment, *J. geophys. Res.,* **73**, 7089–7105.

Métivier, L., Greff-Lefftz, M. & Altamimi, Z., 2010. On secular geocenter motion: the impact of climate changes, *Earth planet. Sci. Lett.,* **296**, 360–366.

Nield, G.A., Whitehouse, P.L., King, M.A., Clarke, P.J. & Bentley, M.J., 2012. Increased ice loading in the Antarctic Peninsula since the 1850s and its effect on glacial isostatic adjustment, *Geophys. Res. Lett.,* **39**, L17504, doi:10.1029/2012GL052559.

Parrenin, F. *et al.* 2007. 1-D-ice flow modelling at EPICA Dome C and Dome Fuji, East Antarctica, *Clim. Past.,* **3**, 243–259.

Paulson, A., Zhong, S. & Wahr, J., 2007. Inference of mantle viscosity from GRACE and relative sea level data, *Geophys. J. Int.,* **171**, 497–508.

Peltier, W.R., 1984. The thickness of the continental lithosphere, *J. geophys. Res.,* **89**, 1303–1316.

Peltier, W.R., 1986. Postglacial rebound and transient lower mantle rheology, *Geophys. J. R. astr. Soc.,* **87**, 79–116.

Peltier, W.R., 1996. Mantle viscosity and ice-age sheet topography, *Science,* **273**, 1359–1364.

Peltier, W.R., 1998. Postglacial variations in the level of the sea: Implications for climate dynamics and solid-Earth geophysics, *Rev. Geophys.,* **36**, 603–689.

Peltier, W.R., 1999. Global sea level rise and glacial isostatic adjustment, *Glob. planet. Change,* **20**, 92–123.

Peltier, W.R., 2002. Global glacial isostatic adjustment: palaeogeodetic and space-geodetic tests of the ICE-4G (VM2) model, *J. Quat. Sci.,* **17**, 491–510.

Peltier, W.R., 2004. Global glacial isostasy and the surface of the ice-age Earth: the ICE-5G (VM2) Model and GRACE, *Annu. Rev. Earth planet. Sci.,* **32**, 111–149.

Peltier, W.R., 2007. History of Earth rotation, in *Treatise on Geophysics, Evolution of the Earth,* Vol. **9**, pp. 243–293, ed. Stevenson, D., Elsevier Press.

Peltier, W.R., 2009. Closure of the budget of global sea level rise over the GRACE era: the importance and magnitudes of the required corrections for global glacial isostatic adjustment, *Quat. Sci. Rev.,* **28**, 1658–1674.

Peltier, W.R. & Drummond, R., 2008. Rheological stratification of the lithosphere: a direct inference based upon the geodetically observed pattern of the glacial isostatic adjustment of the North American continent, *Geophys. Res. Lett.,* **35**(16), L16314, doi:10.1029/2008GL034586.

Peltier, W.R. & Fairbanks, R.G., 2006. Global glacial ice volume and Last Glacial Maximum duration from an extended Barbados sea level record, *Quat. Sci. Rev.,* **25**, 3322–3337.

Peltier, W.R., Argus, D.F. & Drummond, R., 2014. ICE-6G_C (VM5a): a revised model of postglacial rebound fit to geologic and space geodetic data, submitted.

Peltier, W.R., Drummond, R. & Roy, K., 2012. Comment on "Ocean mass from GRACE and glacial isostatic adjustment" by D. P. Chambers et al., *J. geophys. Res.* **117**, B11403, doi:10.1029/2011JB008967.

Peltier, W.R., Shennan, I., Drummond, R. & Horton, B., 2002. On the postglacial isostatic adjustment of the British Isles and the shallow viscoelastic structure of the Earth, *Geophys. J. Int.,* **148**, 443–475.

Petit, G. & Luzum, B., 2010. *IERS Conventions, 2010. Verlag des Bundesamts für Kartographie und Geodäsie,* Frankfurt am Main.

Riva, R.E.M. *et al.*, 2009. Glacial Isostatic Adjustment over Antarctica from combined ICESat and GRACE satellite data, *Earth planet. Sci. Lett.,* **288**, 516–523.

Rott, H., Rack, W., Nagler, T. & Skvarca, P., 1998. Climatically induced retreat and collapse of northern Larsen Ice Shelf, Antarctic Peninsula, *Ann. Glac.,* **27**, 86–92.

Rott, H., Rack, W., Skvarca, P. & De Angelis, H., 2002. Northern Larsen Ice Shelf, Antarctica: further retreat after collapse, *Ann. Glac.,* **34**, 277–282.

Rutt, I.C., Hagdorn, M., Hulton, N.R.J. & Payne, A.J., 2009. The Glimmer community ice sheet model, *J. geophys. Res.,* **114**, F02004, doi:10.1029/2008JF001015.

Schmid, R., Collilieux, X., Dilssner, F., Dach, R. & Schmitz, M., 2010. Updated phase center corrections for satellite and receiver antennas, in *Paper Presented at IGS Workshop*, *Int. GNSS Serv.,* Newcastle, U.K.

Shepherd, A. *et al.*, 2012. A reconciled estimate of ice-sheet mass balance, *Science,* **338**, 1183–1189.

Sibthorpe, A., Weiss, J.P., Harvey, N., Kuang, D. & Bar-Sever, Y., 2010. Empirical modeling of solar radiation pressure forces affecting GPS satellites, *Abstract G54A-04 presented at 2010 Fall Meeting, American Geophysical Union,* Dec. 13–17, San Francisco, CA.

Simon, K.M., James, T.S. & Ivins, E.R., 2010. Ocean loading effects on the prediction of Antarctic glacial isostatic uplift and gravity rates, *J. Geodesy.,* **84**, 305–317.

Sjöberg, L., Walyeldeen, H. & Horemuz, M., 2011. Estimation of crustal motions at the permanent GPS station SVEA, Antarctica from 2005 to 2009, *J. Geod. Sci.,* **1,** 215–219.

Stanford, J.D., Hemingway, R., Rohling, E.J., Challenor, P.G., Medina-Elizalde, M. & Lester, A.J., 2011. Sea-level probability for the last deglaciation: a statistical analysis of far-field records, *Glob. planet. Change,* **79,** 193–203.

Swenson, S., Chambers, D. & Wahr, J., 2008. Estimating geocenter variations from a combination of GRACE and ocean model output, *J. geophys. Res.,* **113,** B08410, doi:10.1029/2007JB005338.

Tarasov, L. & Peltier, W.R., 1997. Terminating the 100 kyr ice age cycle, *J. geophys. Res.,* **102**(D18), 21 665–21 693.

Tarasov, L. & Peltier, W.R., 1999. Impact of thermomechanical ice sheet coupling on a model of the 100 kyr ice age cycle, *J. geophys. Res.,* **104,** 9517–9545.

Tarasov, L. & Peltier, W.R., 2002. Greenland glacial history and local geo-dynamic consequences, *Geophys. J. Int.,* **150,** 198–229.

Tarasov, L. & Peltier, W.R., 2003. Greenland glacial history, bore-hole constraints, and Eemian extent, *J. geophys. Res.,* **108**(B3), 2143, doi:10.1029/2001JB001731.

Tarasov, L., Dyke, A.S., Neal, R.M. & Peltier, W.R., 2012. A data-calibrated distribution of deglacial chronologies for the North American ice complex from glaciological modeling, *Earth planet. Sci. Lett.,* **315,** 30–40.

Thomas, I.D. *et al.*, 2011. Widespread low rates of Antarctic glacial iso-static adjustment revealed by GPS observations, *Geophys. Res. Lett.,* **38,** L22302, doi:10.1029/2011GL049277.

Tregoning, P., Burgette, R., McClusky, S.C., Lejeune, S., Watson, C.S. & McQueen, H., 2013. A decade of horizontal deformation from great earthquakes, *J. geophys. Res.,* **118,** 1–11.

Turcotte, D.L. & Schubert, G., 2002. Geodynamics, Cambridge Univ. Press.

Tushingham, A.M. & Peltier, W.R., 1991. ICE-3G—a new global model of late Pleistocene deglaciation based upon geophysical predictions of postglacial relative sea-level change, *J. geophys. Res.,* **96**(B3), 4497–4523.

Velicogna, I. & Wahr, J., 2006. Measurements of time-variable gravity show mass loss in Antarctica, *Science,* **311,** 1754–1756.

Wahr, J., Molenaar, M. & Bryan, F., 1998. Time variability of the Earth‘s gravity field: hydrological and oceanic effects and their possible detection using GRACE, *J. geophys. Res.,* **103**(B12), 30 205–30 229.

Whitehouse, P.L., Bentley, M.J. & Le Brocq, A.M., 2012a. A deglacial model for Antarctica: geological constraints and glaciological modelling as a basis for a new model of Antarctic glacial isostatic adjustment, *Quat. Sci. Rev.,* **32,** 1–24.

Whitehouse, P.L., Bentley, M.J., Milne, G.A., King, M. & Thomas, I.D. 2012b. A new glacial isostatic adjustment model for Antarctica: calibrated and tested using observations of relative sea-level change and present-day uplift rates, *Geophys. J. Int.,* **190,** 1464–1482.

Wu, X., Collilieux, X., Altamimi, Z., Vermeersen, B.L.A., Gross, R.S. & Fukumori, I. 2011. Accuracy of the International Terrestrial Reference Frame origin and Earth expansion, *Geophys. Res. Lett.,* **38,** L13304, doi:10.1029/2011GL047450.

Zanutta, A., Vittuari, L. & Gandolfi, S., 2008. Geodetic GPS-based analysis of recent crustal motions in Victoria Land (Antarctica), *Glob. planet. Change,* **62,** 115–131.

SUPPORTING INFORMATION

Additional Supporting Information may be found in the online version of this article:

Figure S1. Estimates as a function of time of Earth's scale in transformations from JPL's GPS solution into the constant rate in ITRF2008. The series for JPL's GPS solution determined 3 yr ago (Desai *et al.* 2009) is crooked. The series for JPL's determined 18 months ago (Desai *et al.* 2011) is straight. Using data decimation and spectral analysis, Argus (2012) estimate uncertainty in scale rate to be reduced by 40 per cent.

Figure S2. Estimates of position as a function of time of permanent GPS sites in Antarctica and on Kerguelen island. Position estimates are either used (light blue dots), omitted as outliers (red dots), or omitted due to antenna malfunction (pink dots). The model (dark blue curve) consists of a velocity, a sinusoid with a period of 1 yr, and offsets (vertical line segments) either at (blue) or not at (red) the time of logged antenna substitutions. (Vertical line segments along the horizontal axis are possible offsets that we do not estimate.) At top left is the rate in millimetres per year. At top right is the peak-to-peak amplitude of the sinusoid and the time of maximum vertical position. The phase of the sinusoid is constrained to be identical for all three components. At bottom left is the root mean square misfit in mm. At bottom right is the effective time period of observation in years. At the very bottom the X's mark the times of logged antenna substitutions in the IGS and SIO log files and the Y's mark the times of offsets in ITRF2008. To show or evaluate the change in velocity at sites PALM, OHI2, OHI3 and ROTB, we show alternative velocities (in orange and brown) fit to non-overlapping parts of the time period of observations. *Notes:* We estimate *Vesleskarvet* to be rising at 1.5 mm yr^{-1} without estimating an offset. If we were to estimate an offset in 2008 April, we would find the offset to be 8 mm in the vertical, the root mean square misfit decreases by 4 per cent, and uplift to increase 0.7 mm yr^{-1}. Choosing whether to estimate this offset, which is not at the time of a logged antenna substitution, is a close call. (In Argus *et al.* 2011 we estimated uplift to be 2 mm yr^{-1} faster, partly because we estimated an offset of 13 mm.) We estimate *Syowa* to be rising at 0.5 mm yr^{-1}, estimating a vertical offset of 13 mm in 2000 January. Estimating this offset reduced the root mean square misfit by 12 per cent. If we were to estimate an offset in 2007 January, we would find the offset to be 6 mm in the vertical, root mean square misfit to decrease by 3 per cent, and uplift to increase by 0.7 mm yr^{-1}. (In Argus *et al.* 2011 we estimated uplift to be 2 mm yr^{-1} faster because we had estimated the 2007 January offset but not the 2000 January offset.) We estimate *Casey* to be rising at 1.8 mm yr^{-1}, estimating a vertical offset of 8 mm in 2009 October. Estimating this offset reduces the root mean square misfit by 6 per cent. Six months of anomalous data in 1997 were discarded. Choosing whether to estimate this offset not at the time of an antenna substitution is a close call. We estimate *Davis* to be subsiding at 0.9 mm yr^{-1}, solving for three offsets at the time of antenna substitutions. We estimate the 1999 November east offset to be 3 mm. Estimating this offset reduces the root mean square misfit by 5 per cent. Whether to estimate this offset was a close call.

Figure S3. Estimates of position as a function of time of GPS sites in the West Antarctic interior with campaign WAGN and permanent ANET data at the same mark. The campaign observations (blue circles) are connected to the succeeding permanent observations (in pink). Small pink dots show all the permanent positions; red circles show permanent observations on the 1st and 16th day of the month. We fit a velocity to the campaign data and only the permanent positions on the 1st and 16th day of the month. If we were to fit all the data, we would find the velocity poorly fits the campaign data because the permanent data would be weighted too heavily. (See Fig. 9 of the main text.) See Fig. S2 for a complete description of symbols and values given.

Figure S4. Estimates of the velocity of Earth's centre, the point relative to which vertical rates of site motion are estimated. The velocity of Earth's centre also defines the translational velocity of Earth's reference frame. *X* is in the direction of the geocentric vector to 0°N 0°E, *Y* is towards 0°N 90°E and *Z* is toward 90°N. (a) The velocity of (CM) the centre of mass of Earth, oceans and

atmosphere in ITRF2000, ITRF2005 and ITRF2008. At the origin is the velocity of CM estimated from SLR in ITRF2008 (beige—filled 95% confidence limits; Altamimi *et al.* 2011). Also plotted is the velocity of CM estimated from GPS by JPL (green—filled 95% confidence limits; Desai *et al.* 2011; Argus 2012). (b) Two estimates of the velocity of CE determined from horizontal site velocities by assuming places on the plate interiors not near ice sheets have, besides plate motion, negligible horizontal motion relative to CE. Blue ellipse—from this study's data, pink ellipse—from the ITRF2008 site velocities. Also plotted is the estimate of Altamimi *et al.* (2012) from the ITRF2008 site velocities. (c) Three estimates of the velocity of CE determined from vertical rates of site motion. Places on the plate interiors not near ice sheets are assumed to move vertically as predicted by a postglacial rebound model. Blue ellipse—from this study's data, correcting for ICE–6G (VM5a), yellow ellipse—from this study's data, correcting for the postglacial rebound model of A *et al.* (2013). Pink ellipse—from the ITRF2008 site velocities, correcting for ICE–6G (VM5a). Also plotted is the estimate of Bevis *et al.* (2013) determined by assuming places not near ice sheets have no vertical motion. (d) Three estimates of the velocity of CE determined from vertical and horizontal site velocities. The assumptions in both (b) and (c) are made. Also plotted is the (hexagon) estimate of Wu *et al.* (2011) from GPS, GRACE gravity and ocean bottom pressure data.

Figure S5. The horizontal predictions of ICE-6G_C (VM5a; left-hand side) are compared with the horizontal observations in the ICE-6G_C (VM5a) reference frame (right-hand side). The horizontal velocities in the ICE-6G_C (VM5a) frame are the sum of the horizontal residuals relative to ICE-6G_C (VM5a) and the horizontal predictions of the rotational feedback component of the ICE-6G_C (VM5a).

Figure S6. Ice loss as a function of time in the Northern Antarctica Peninsula and in the Amundsen Sea sector of West Antarctica estimated using GRACE gravity observations from 2003 January to 2013 February. The kernels over which gravity decrease was averaged are shown in Fig. S7. Estimates of ice loss are not corrected for a postglacial rebound model. The mean rates of ice loss in the Northern Antarctica Peninusla (-28 Gt yr^{-1}) and in the Amundsen Sea sector (-124 Gt yr^{-1}) were used to construct the models of current ice loss in Fig. S7. The GRACE Release 5, GSM solution from CSR was used. The GSM spherical harmonic coefficients were expanded to determine surface mass (Wahr *et al.* 1998). We added the degree-1 coefficients estimated from GRACE and ocean models by Swenson *et al.* (2008). The C20 values estimated from SLR were used. A Gaussian smoothing factor of 220 km was applied to reduce errors at high spherical harmonic degree (Wahr *et al.* 1998). Chen *et al.* (2009) and Horwath & Dietrich (2009) have also evaluated current Antarctic ice loss using GRACE.

Figure S7. Our elastic model of current ice loss near Pine Island Bay and in the Northern Antarctica Peninsula is constructed from mass loss inferred from GRACE (see Fig. S6) and mass gain due to uplift in ICE-6G_C VM5a. (Top left) Vertical motion inferred from GRACE gravity observations from 2003 January to 2013 February calculated from Kusche & Schrama (2005). Local maxima are 6 mm yr^{-1} near Pine Island Bay and 2 mm yr^{-1} near the tip of the Antarctica Peninsula. These estimates far understate the true uplift maxima because GRACE smears out the signal over a broad area. The blue and pink X's show the kernels used to estimate mass loss in, respectively, the Northern Antarctic Peninsula and near Pine Island Bay (Fig. S6). See Fig. S6 for specifics on the GRACE observations. (Bottom left) Change in equivalent water thickness inferred from the same GRACE data. Maxima and minima are given in mm yr^{-1}. (Top right) Vertical motion in our elastic model of current ice loss. Current ice loss of -143 Gt yr^{-1} near Pine Island Bay is calculated from the mass loss inferred from GRACE (-124 Gt yr^{-1}) and the mass gain due to uplift in ICE-6G_C VM5a (19 Gt yr^{-1}). Current ice loss of -40 Gt yr^{-1} in the Northern Antarctic Peninsula is calculated from the mass loss inferred from GR (-28 Gt yr^{-1}) and the mass gain due to uplift in ICE-6G_C VM5a (12 Gt yr^{-1}). The X's show the locations of the evenly spaced disks used to construct the model. The ice loss inferred from GRACE and ICE-6G_C VM5a is distributed evenly over the X's. Each disk has a radius of 63 km, the value that exactly fills the area between the X's. Near Pine Island Bay our model predicts uplift at 26 mm yr^{-1}, at roughly the rates of 18–28 mm yr^{-1} observed at three GPS sites (Groh *et al.* 2012). In the Northern Peninsula our model predicts uplift at 7 mm yr^{-1}, at roughly half the maximum rate observed (Table 1). While we do not attempt to fit the spatial detail of uplift near Pine Island Bay and in the Northern Antarctica Peninsula, our model of current ice loss provides accurate predictions of uplift outside of these two areas. (Bottom right) Change in equivalent water thickness in our elastic model of current ice loss. Equivalent water thickness decreases by -0.96 m yr^{-1} over a 74 800 km^2 area near Pine Island Bay (6 X's) and by -0.26 m over a 74 800 km^2 area in the Northern Antarctica Peninsula (6 X's).

Figure S8. Uplift predicted by two elastic models of current ice loss. (Top) This study's model constructed on the basis on CSR GRACE data from 2003 to 2012 and corrected for postglacial rebound model ICE-6G VM5a. (Bottom) The alternative elastic model of Thomas *et al.* (2011, supplementary text) based on ICESat data from Riva *et al.* (2009; R.E.M. Riva and M. A. King, personal comm., 2013).

Figure S9. Ice thickness at the Last Glacial maximum relative to the Present in ICE-6G_C. Changes in ice thickness at 12, 11, 8 and 5 ka relative to the Present in iCE-6G.

Figure S10. Total topography at Last Glacial Maximum 26 ka. Total topography equals bedrock elevation plus ice thickness in ICE-6G_C (http://gji.oxfordjournals.org/lookup/suppl/doi:10.1093/gji/ggu140/-/DC1).

Please note: Oxford University Press is not responsible for the content or functionality of any supporting materials supplied by the authors. Any queries (other than missing material) should be directed to the corresponding author for the article.